BOREHOLE GEOLOGY AND HYDROTHERMAL MINERALISATION OF WELLS MW-01 AND MW-02, MENENGAI GEOTHERMAL FIELD, CENTRAL KENYA RIFT VALLEY

Convine Omondi
Geothermal Development Company, Ltd. – GDC
P.O. Box 17700-20100
Nakuru
KENYA
comondi@gdc.co.ke, convineomondi@yahoo.com

ABSTRACT

MW-01 and MW-02 are geothermal exploration wells located on the Menengai caldera floor. They are both vertical wells, drilled to a total measured depth of 2206 m (MW-01) and 3200 m (MW-02). This report presents a study of the drill cuttings which were taken at 2 m intervals from the 2206 m in well MW-01 and the upper 2156 m in MW-02. The Menengai lithology is largely peralkaline silica saturated trachytes. MW-01 penetrated a massive fine- to- medium grained pantelleritic trachyte sequence while MW-02 cut more evolved rocks, comprising largely of rhyolitic trachytes, minor pantelleritic trachytes, comendites and comenditic trachytes. A pantelleritic intrusive body exists between 850-1082 m and at 2196 m in MW-01 whereas a possible comendite intrusion exists below 1952 m. No apparent stratigraphic correlations between the two wells are evident. Temperature logs from the wells indicate two main feed zones in MW-01 at 750-800 m and at 1900-2000 m, but in MW-02 minor feed zones are found at 400-600 and 1100-1300 m. Feed zones associated with circulation loss zones appear at lithological boundaries and adjacent to intrusive bodies. The upper feed zones in each well seem to have low temperatures leading to cooling effects at the bottom of the wells. Hydrothermal alteration is influenced by the rock chemistry, temperature and permeability. The main index mineral is epidote, indicating minimum alteration temperatures of 240-250°C. Epidote was first noted at 1090 m in MW-01 and at about 1500 m in MW-02. Smectite, chlorite and mixed-layer clay minerals are conspicuously minor or completely absent, while illite is found in both wells. More research is, therefore, required to outline the indicators for the alteration zone system and the mineralogical evolutionary sequence. A comparison of fluid inclusion homogenization temperatures with the estimated formation and alteration temperatures indicates reservoir temperatures between 230 and 280°C and a state of equilibrium. The present Menengai caldera is the result of collapses of mini-caldera segments along criss-crossing fractures on the floor of the main caldera. These fractures could contribute greatly to the localised recharge of the geothermal system, originating from the underlying intra-caldera lake situated in the northeast part of the caldera.

1. INTRODUCTION

1.1 General information

Wells MW-01 and MW-02 are the first geothermal exploration wells at the Menengai prospect, drilled by the Geothermal Development Company (GDC) of Kenya. They both lie on the floor of the Menengai caldera at Eastings 171846.9 and 171597.2, respectively, and Northings 9976848.9 and 9979477.7, respectively. The prospect's coverage is expansive, extending to the northwest, covering the Ol´Rongai and Ol´Banita high-temperature fields. Geothermal development in Kenya is currently enjoying a massive increase following the ever growing electricity demand with the growing population. At present, only the Olkaria geothermal field is being exploited with an average production of 210 MWe (Ouma, 2010). GDC, a creation of the Government of Kenya, was mandated to carry out geothermal exploration and development in the Menengai area.

1.2 Objective of the study

The aim of this project is to study the borehole geology of the first two Menengai wells by analysing drill cutting samples taken at 2 m intervals in both wells in order to identify the subsurface formations, locate aquifers or feed zones, determine the alteration and hydrothermal indicator minerals and try to conceptualize the geothermal systems and temperatures in the Menengai prospect.

This project report was prepared and submitted as a requirement for the fulfilment and attainment of a six month Postgraduate course on Borehole Geology at the United Nations University Geothermal Training Programme (UNU-GTP) in the period between May and October 2011.

1.3 Methodology

Drill cuttings from wells MW-01 and MW-02 to depths of 2206 m and 2156 m, respectively, were analysed with the help of a binocular microscope. Other analyses included: petrographic analysis of 40 thin sections from different depths in well MW-01, fluid inclusion analysis of selected samples at 7 depth locations in MW-01 and 2 locations in MW-02, and X-ray diffractometer analysis of 30 samples at selected depth locations. Temperature logs were also interpreted. A correlation of the findings from the above analyses between the wells was carried out in an attempt to interrelate the lithostratigraphy, geological structures and the nature of the geothermal system at these two locations.

2. REGIONAL GEOLOGY AND TECTONIC SETTING

2.1 Regional geology

The regional surface geology of Menengai is largely composed of late Quaternary volcanics (Figure 1). The area north of Menengai is characterised by lavas from N-S trending fissures. The lavas are trachytic and trachy-phonolitic in composition, mainly observed at, and exposed by, the scarp walls beyond the Ol´banita swamps, Lomolo and Kisanana areas (GDC, 2010). They underlie ignimbrites and pyroclastics, probably originating from Menengai eruptions to the south. Basaltic lavas dominate the Solai axis. Ol´Banita and Ol´Rongai areas, which are low-lying, are covered with thick soils derived mainly from pyroclastics and extensive thick ignimbrite beds from the caldera. Ol´Rongai ridge rises to 2100 m a.s.l., approximately 400 m above the general altitude of the surrounding area. Eruptions here vary from fissure gas-poor trachytic lavas to highly explosive gas-rich volcanic ash and pumice (GDC, 2010).

The caldera and its immediate surroundings are characterised by pre-caldera trachytic lavas, largely exposed in the caldera walls, syn-caldera ignimbrite at the eastern and northern rims and agglomeratic deposits of poorly sorted angular lithic and glassy/semi-pumiceous ash materials (GDC, 2010). Extensive upwelling of the ground north and west of the caldera (Kampi ya moto, El bonwal and Ol´Rongai) may have occurred in syn-caldera times as well. Here, the ignimbrite resembles welded tuff with numerous collapsed pumice materials, thinning away to the north and east; it occurs as tuff representing distal facies (GDC, 2010).
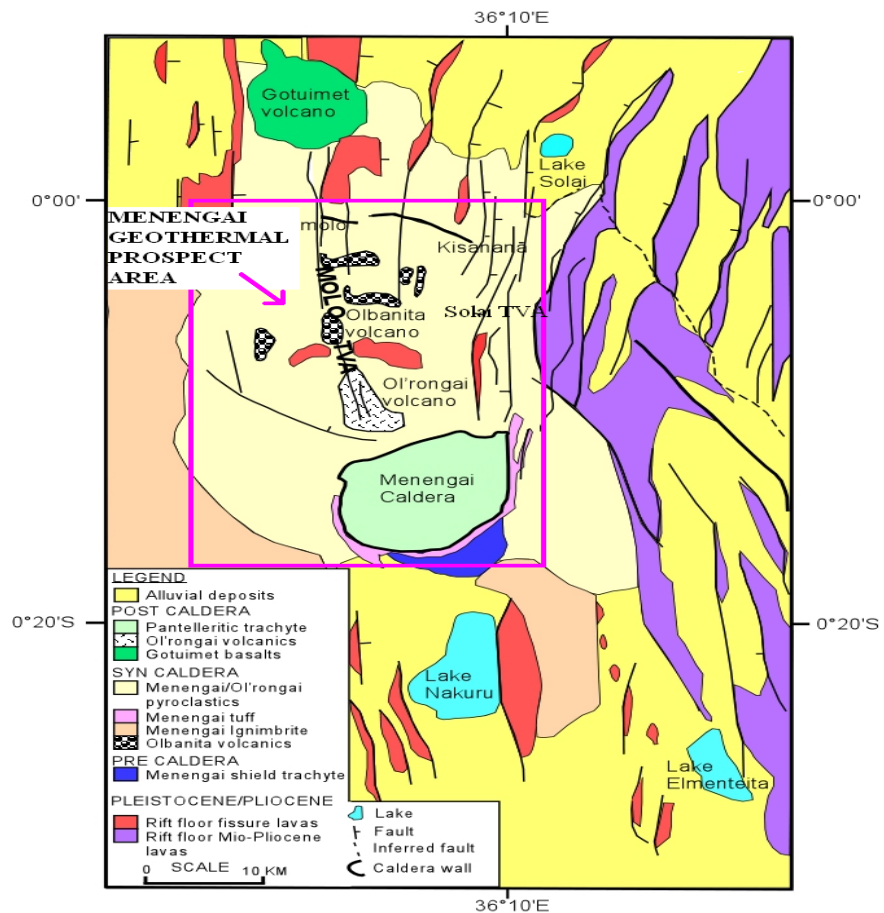

FIGURE 1: Regional surface geological map (GDC, 2010)

Post-caldera materials are mainly composed of lavas which are largely found on the caldera floor in addition to minor eruption centres to the southwest of the volcano. These eruptive materials were preceded by explosive episodes of ash and pumice cinder cones and tephra sheets onto the caldera floor (Leat, 1984). Intra-caldera lake sediments of well bedded pumiceous sands with rounded pebbles in the northeast part of the caldera floor (Figure 2) indicates the existence of a paleo-lake believed to be the result of overflow from the 'Gamblian' lake (Figure 2) into the caldera through the southeast graben and partly through underground channels, along joints and through tephra and soil horizons (Leat, 1984).

2.2 Tectonic setting

The Kenya Rift Valley is a segment of the eastern arm of the East African Rift System (EARS). It extends from Lake
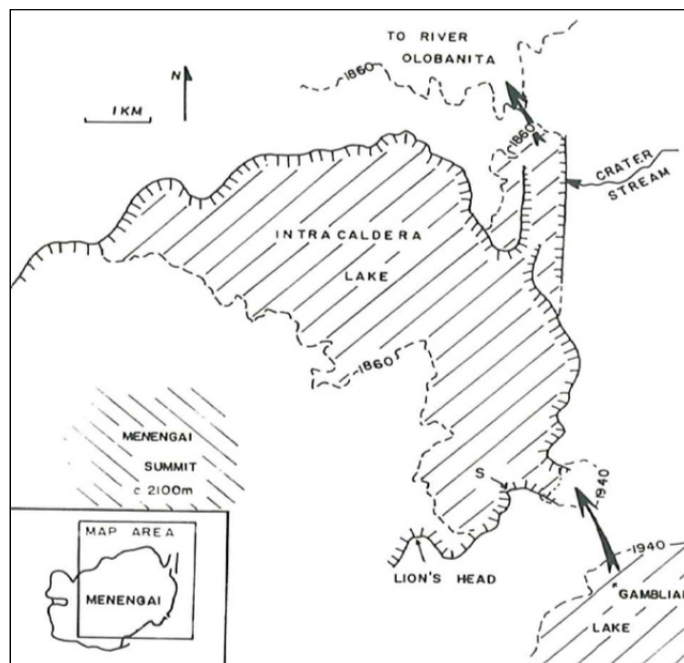

FIGURE 2: Intra-caldera lake sediments (diagonal lines); Arrows indicate probable water flow directions into and out of the caldera (Leat, 1984)
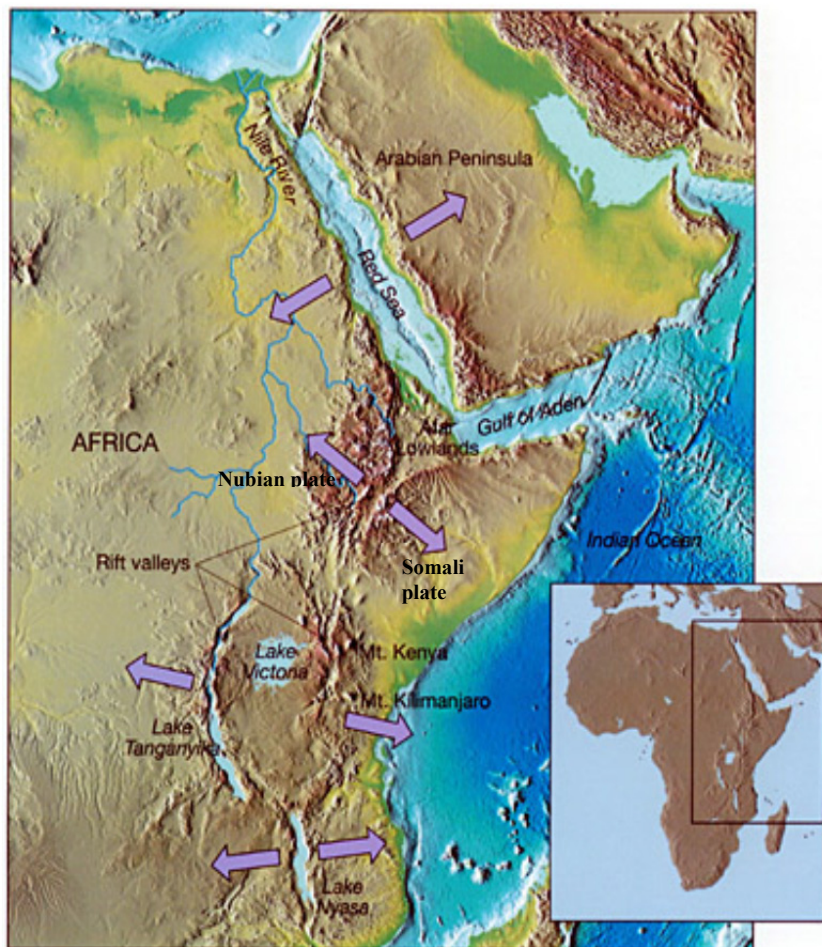
FIGURE 3: East African Rift System (EARS)
(modified from GDC, 2010)

Turkana in the north to Lake Natron, lying at the Kenya-Tanzania border in the south. The EARS (Figure 3) is an active continental divergent plate boundary at which the African plate is splitting into the Nubian and Somali proto plates and has undergone massive volcanism from the late Tertiary to Recent. It runs more than 5000 km from the Gulf of Aden to Mozambique. The Kenya Rift segment became active about 30 million years ago (Oligocene) in the Lake Turkana area (dubbed the Turkana rift) to the north and subsequently propagated southwards with increasing activity about 14 million years ago (Baker and Wohlenberg, 1971; Baker et al., 1972).

These tectonics led to the formation of a graben structure (approx. 5 M years ago) with an average width of 40-80 km followed by fissure eruptions in the axis of the rift to form flood lavas, 2-1 M years ago, leading to the development of massive large shield volcanoes along the fissures and axes of the rift, some examples being Suswa, Longonot, Ol´Karia, Eburru, Menengai, Korosi, Paka, Silali, Emuruangogolak, and Barrier volcanic complexes (Figure 4). Most of these volcanic centres have undergone one or more explosive eruption phases leading to caldera collapses. The volcanic centres are dotted by surface hydrothermal alteration and indicators envisaged to host geothermal systems driven by hot magmatic intrusions.

2.3 Menengai volcanic complex

Menengai is a massive, relatively young (<0.2 Ma) caldera volcano located in the south-central Kenya Rift Valley (Figure 4). Leat (1984, 1991) and Jones (1985) described the geology of the Menengai volcano. It is classified as a shield-volcano and K-Ar analyses date it back to 0.18 ± 0.01 M years. Subordinate pyroclastics include strombolian-style cinder cones, which form the northwest part of the shield, and plinian-style pumice falls, which were erupted in late pre-caldera times. Syn-caldera activity is represented by two ash flow tuffs, which were both preceded by pumice falls (Leat, 1984, 1991). The first (representing about 20 km^3 of magma) is separated from the second (representing about 30 km^3 of magma) by sediments up to 4 m thick. Both ash flows were emplaced as single flow units and have outflow sheet aspect ratios of about 1:4,000. Half the volume of the combined ash flow sheet was ponded in the caldera (Leat, 1984, 1991).

The present caldera (12 × 8 km) formed in association with the eruption of the second ash flow tuff (Leat 1984). A well-developed sector graben, embayed caldera walls, and apparently random spacing

of some post caldera vents indicate a segmental collapse. Twenty-three cubic kilometres of magma were erupted as more than 70 post caldera lava flows which cover the caldera floor. Cinder cones are rare and plinian-style pumice falls represent about 2 km^3 of magma. Most lavas and pumice falls were erupted from vents located near the centre of the caldera (Leat, 1984, 1991). Correlations of Menengai volcanics with the nearby fluctuated soda lakes indicated an age of 29,000 years and about 14,000 years for the eruptions of the two ash flows, respectively (Leat, 1984). Intra-caldera lake sediments prove the existence of a lake (from 10,300 to 8,300 years B.P.) with a prominent phreatomagmatic deposit, the Ruplax tuff.

Isopach maps for the pre-caldera volcanics (Figure 5) illustrate that the volcano was shield-like, with flanks dipping 1.5-8° away from the summit and had a broadly oval plan, with a major axis of 22 km, trending NW-SE, and a minor axis of 15 km trending NE-SW (Leat 1984). It had a maximum thickness of just over 300 m, covered an area of approx. 210 km^2 and probably had a central ridge (Figure 5) lying along the major axis, with a line of vents along the crest. This central ridge would have intersected the regional approximately 45° fault trend (Leat 1984). It is at this intersection that the caldera collapse occurred (Figure 5).

2.4 Geological, geophysical and geochemical characteristics of the Menengai Volcano

Menengai is composed almost entirely of strongly quartz-normative, silica-oversaturated, peralkaline trachytes, with subordinate volumes of metaluminous trachytes and pantelleritic rhyolites (Macdonald et al., 1970; 1994; 2011; Macdonald and Bailey, 1973; Macdonald, 1974; Leat et al., 1984; Macdonald and Scaillet, 2006; Macdonald and Baginski, 2009). Macdonald (1974) classified the Menengai rocks as ranging from comenditic trachyte through pantelleritic trachyte to pantellerite based on Al_2O_3 and FeO contents (Section 4.3).

The MW-01 and MW-02 geothermal exploration wells were the first to expose the subsurface rocks of
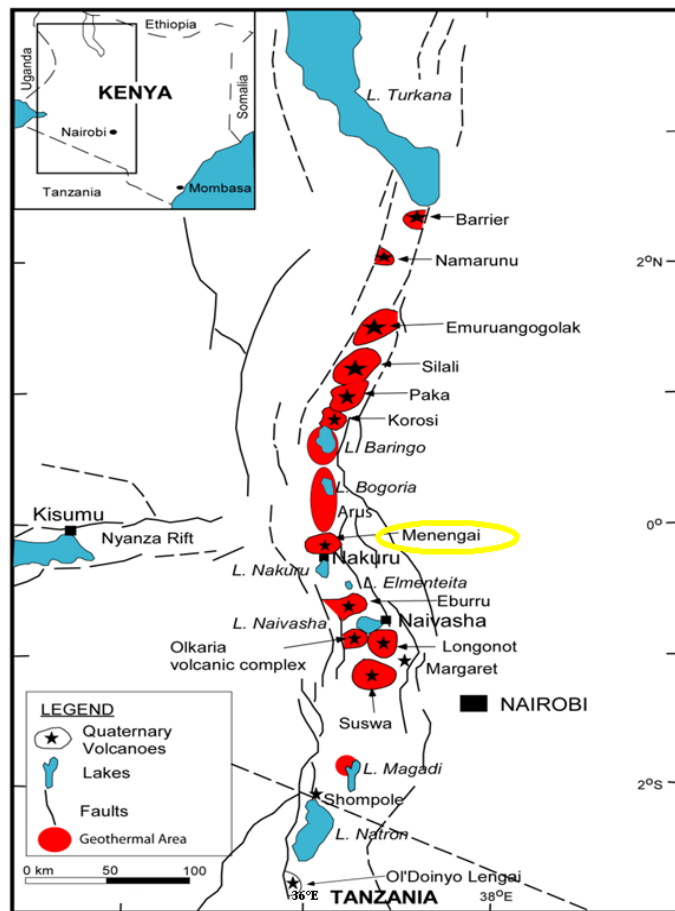
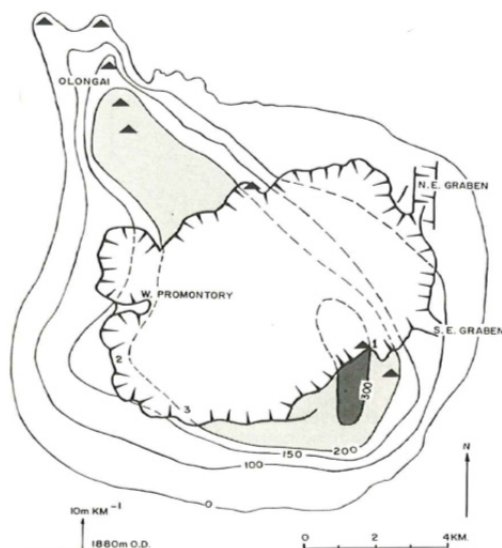FIGURE 4: Major volcanic centres on the Kenya Rift floor (GDC, 2010)

FIGURE 5: Isopach map for the pre-caldera volcanics of Menengai; solid triangles indicate probable or possible pre-caldera vents; point 1 – the Lion´s head cliff; point 2 – the west cliff; and point 3 - the southwest cliff (Leat, 1984)

Menengai. MW-01 saw a series of compositional zones of fresh pantelleritic trachyte with surbordinate, thin intercalated trachytic tuffs, while MW-02 encountered more evolved rocks: rhyolites, trachytes, minor pantelleritic trachytes, comendite and comenditic trachyte. MW-01 and MW-02, therefore, probably penetrate lavas of different volcanic episodes, the latter pre-caldera lavas while the former encounters the post-caldera young lavas covering the caldera floor.

Menengai shows a complex geochemical evolution, resulting from the interplay of magma mixing, crystal fractionation and liquid state differentiation (Leat et al., 1984). It forms part of the central Kenya peralkaline province, a unique assemblage of peralkaline salic magmatic systems (Macdonald and Baginski, 2009; Macdonald and Scaillet, 2006). The controlling mechanism at any time was related to the growth stage of the complex, the presence of volatile gradients in the chamber, and the distribution of magma densities in the chamber (Leat et al., 1984).

Prior to major ash flow eruptions, the magma reservoir grew by the addition and mixing of two or more trachytic melts, only slightly different in composition. A volatile-rich cap eventually separated from the lava-forming zone and became compositionally zoned by liquid-state processes (Leat et al., 1984). In late pre-caldera times, trachyte magma was able to penetrate the cap zone, resulting in the eruption of mixed magma (Leat et al., 1984). The first Menengai ash flow tuff was erupted from a compositionally zoned magma chamber which showed strong roofward enrichment in Fe, Mn, Cs, Hf, Nb, Pb, Rb, Ta, Th, U, Y, Zn, Zr, and the REE (including Eu) and probably also Na, Cl, and F, and roofward depletion in Al, Mg, Ca, K, Ti, P, Ba, and Sc (Leat et al., 1984).

Zoning of the magma chamber was achieved by liquid state differentiation, probably involving volatile transfer and thermodiffusion, and minor crystal fractionation (Leat and Macdonald, 1984). After a period of homogenization of the magma remaining in the upper parts of the chamber, the second Menengai ash flow tuff was erupted, with the formation of the present caldera. This unit is also compositionally zoned, although with less observed enrichment factors than the first ash flow. Caldera collapse was followed by convective overturn within the magma chamber and the rise to the roof-zone of a Ba-rich magma from a level not tapped by the ash flow (Leat et al., 1984). Enrichment of volatiles in this zone resulted in the establishment of a stable density interface between an upper, tuff-producing zone, and the lower, lava forming zone.
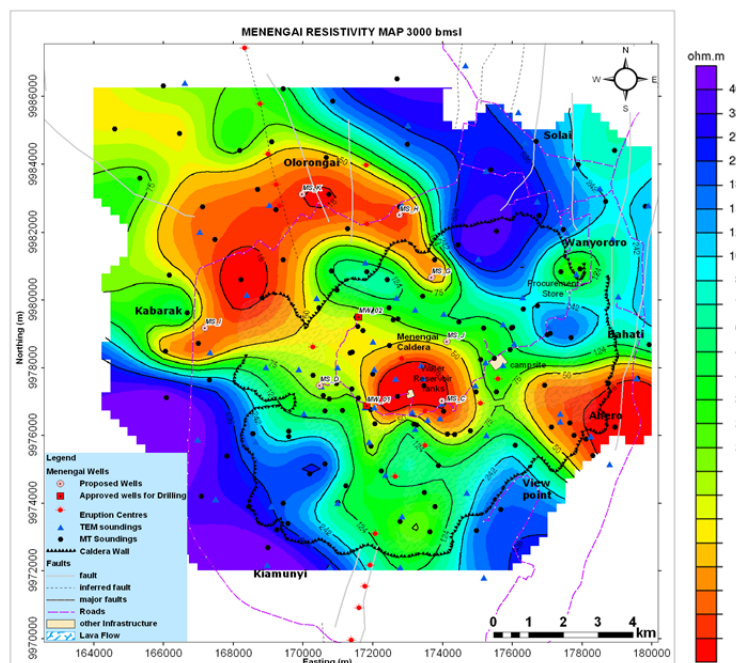

FIGURE 6: Iso-resistivity distribution at 3000 m below sea level in Menengai geothermal prospect (GDC, 2010)

Transient electcromagnetic (TEM) and magnetotelluric (MT) measurements indicate resistivity lows at depths of 5-6 km (Figures 6 and 7) below the surface with a major NW-SE orientation, almost parallel to the main axis of the pre-caldera Menengai shield (Figure 6). Resistivity lows indicate hot intrusions which are probably the heat sources of the geothermal systems. The hot bodies tend to alter the overlying slightly high-resistivity capping layers dominated by hydrothermally altered mineral sequences (GDC, 2010).

Seismic studies (Young et al., 1991; Simiyu and Keller, 2001) indicate that most of the activity is above the depth of 6-7 km in a N-S trending line (Figure 8), as shown by the
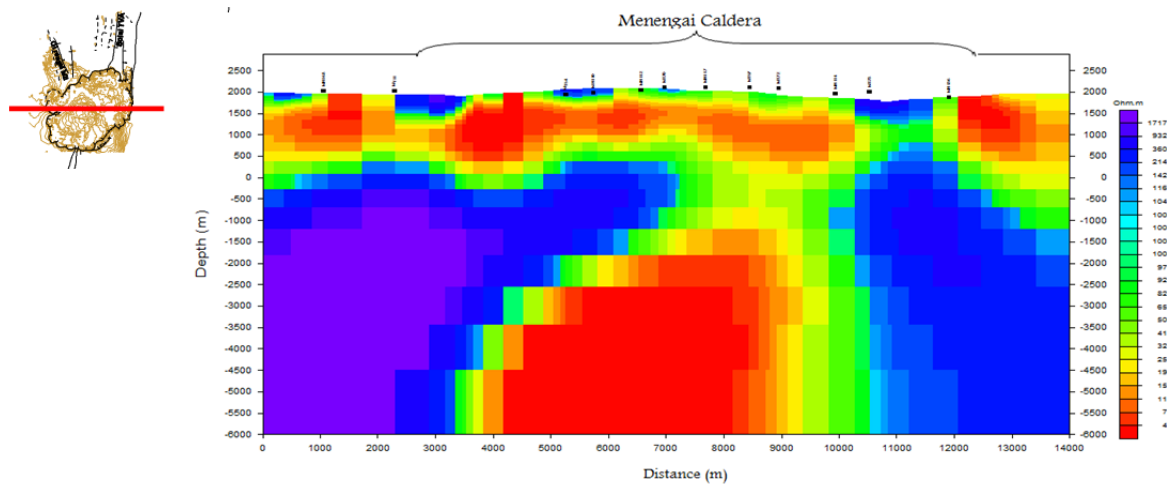
FIGURE 7: Menengai prospect, 2D MT resistivity cross-section trending E-W (GDC, 2010)
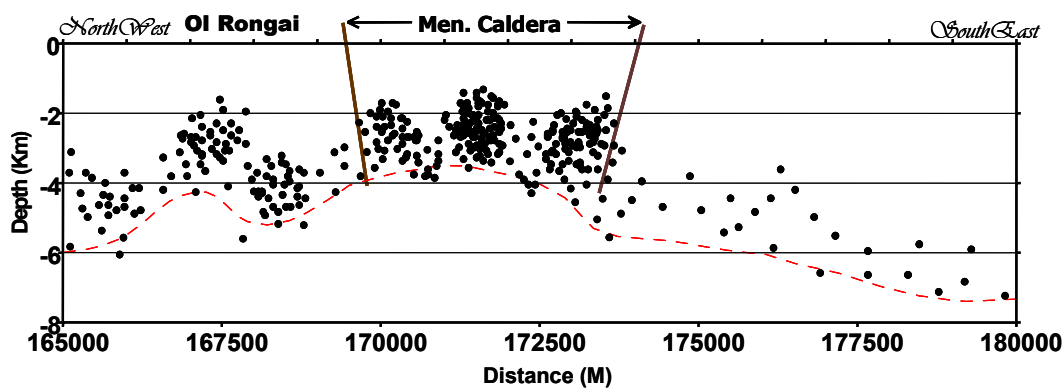

FIGURE 8: Depth distribution of micro-seismic events through Menengai caldera
(Simiyu and Keller, 1997)

seismic attenuation trends coinciding with the princpal direction of the faults (Young et al., 1991; Tongue et al., 1992).

Gravity surveys from the Solai area show a N-S trending anomaly which reaches a maximum in the Molo volcanic axis but is less prominent within the Solai fault zone (Figure 9). This supports the geological observation that the Solai fault zone, despite its relatively intense tectonic activity, is less volcanically active than the Molo axis system due to the fact that it has few eruption centres (GDC, 2010). The resistivity survey identified three zones, separated by discontinuities, which are suitable for geothermal production: the central part of the caldera, which shows a low-resistivity anomaly (<10 Ωm) at depth, the Ol Rongai area, where steaming and dry hot wells are located, an area also showing low resistivity at depth, and the western domain towards Kabarak, which is separated from the central one by a structural discontinuity, and also has a homogenous electrical response and low resistivity (<10 Ωm) (GDC, 2010).

Geochemical analyses indicate high CO_2 values (>1.2%), especially along the fractured zones, with absolute values of Rn-222 indicating a NW-SE trend anomaly. These areas apparently coincide with high Rn-222 absolute values (anomalous values in the range of 2002-3700 cpm) in the caldera and to the north and northwest out of the caldera (GDC, 2010). It also corresponds to high CO_2 values to the northwest of the caldera. Other notable high-ratio values are located east and northeast of the caldera. Mercury concentrations range from 0 to 0.140 mg/m³. According to Arnórsson and Gunnlaugsson (1985) and Nehring and D'Amore (1984) geothermometric functions, based on the concentrations of

CO_2, H_2S and H_2, calculated temperatures on samples from fumaroles show T_{H_2S} geothermometer temperatures in the range of 279-298°C while $T_{H_2S-CO_2}$ ranges between 274 and 304°C.
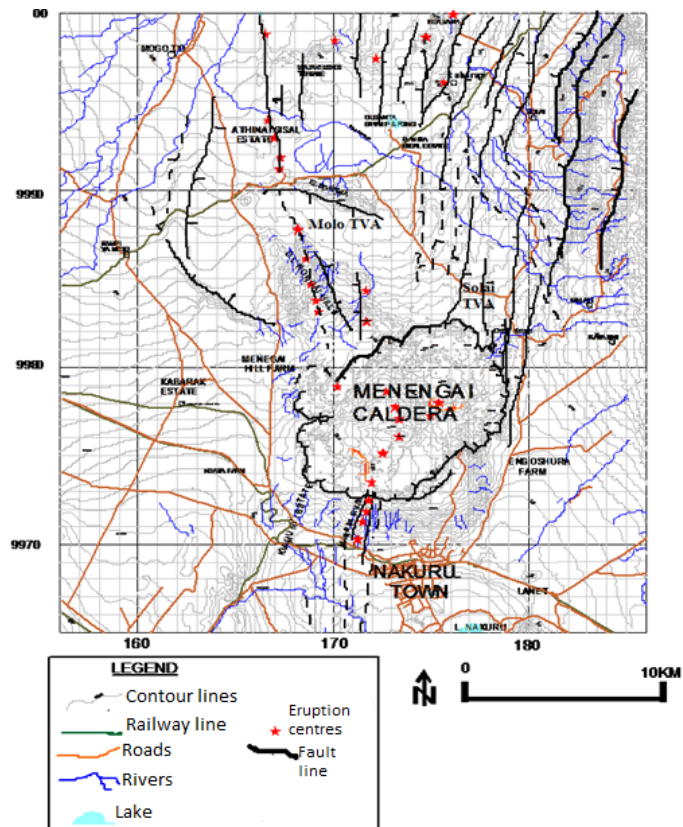

FIGURE 9: Structural map showing orientations of tectonic axes (GDC, 2010)

3. SAMPLING METHODOLOGY AND ANALYSIS

Drill cutting samples from wells MW-01 and MW-02 were collected at every 2 m interval during the drilling operations. Drill cuttings were, however, absent in well sections experiencing total circulation losses. Borehole geologists continuously analysed the well cuttings with the help of a binocular microscope to examine and evaluate the rock stratigraphy and alteration mineral assemblages. Information on the subsurface geology at the drill site also helps to foresee possible imminent problems facing the drilling operations caused by geological factors. This allows swift mitigation measures to be taken in close liaison with the rig crew.

Well cuttings were subsequently taken to the GDC´s geology laboratory in Nakuru where further analyses were undertaken under a binocular microscope to compare with the findings at the rig. The wet cuttings from the rig site were washed to remove dust particles and later dried in electric ovens, archived and stored in clearly labelled containers with lids.

In the present study, drill cuttings of MW-01 down to 2206 m and of MW-02 down to 2156 m were analysed at the Iceland Geosurvey (ISOR) geological laboratories. The samples were further subjected to binocular microscope analysis to identify the lithological units, identify secondary alteration minerals, and evaluate the degrees of alteration in addition to identifying the locations of intrusions. Vein filling and/or fracturing in both wells were revealed as were permeability zones in conjunction with temperature logs. Dilute hydrochloric acid was used to identify the presence of carbonates mainly caused by calcification, keeping in mind though the contributions of external agents like cement.

Forty (40) selected cutting samples from MW-01 were taken for 2 μm thin-section slide preparations for further detailed analysis using a petrographic microscope. This allows the identification of microscopic rock properties like crystallinity, granularity, relative crystal sizes and shapes and orientai

and interstitial textures to help in holistic description and mineral identification in correlation with binocular and visual observations. This also allows further analyses of hydrothermal minerals and the identification of hydrothermal alteration patterns and sequences in veins and vesicle fillings.

Clays analysis of 30 selected cutting samples from well MW-01 and 9 from MW-02 were carried out with the help of an X-ray diffractometer (XRD) to further identify the alteration zones. Here, untreated, glycolated and heated samples were evaluated to classify the clay types found in the wells to find the formation temperatures (Appendix I). Graphical presentations of the results are displayed in Appendix II.

Fluid inclusion analysis of carefully selected secondary quartz from 2 depths in MW-01 was undertaken to predict at which temperatures the minerals formed. Fluid inclusions may provide crucial information on the thermal history of a geothermal system, for example, they can provide evidence as to whether a geothermal system is heating or cooling.

Finally, findings from all the analyses were integrated and compiled using LogPlot 2007 (RockWare Inc., 2007) for ease of conclusive analysis and interpretation.

4. BOREHOLE GEOLOGY

4.1 Drilling at Menengai

Drilling at Menengai commenced in earnest at the beginning of the year 2011. This was done in order to confirm the presence of a geothermal reservoir below the volcanic complex, indicated by surface geological, geophysical and geochemical exploration results (GDC, 2010). Drilling is actively on-going and so far a total of 4 vertical deep exploration wells with a summed average depth of 2500 m b.g.l. have so far been drilled into the caldera floor (Figure 10). MW-01 and MW-02 are subsequently the pioneering exploration wells in the diverse Menengai geothermal prospect located in the central Kenya rift.
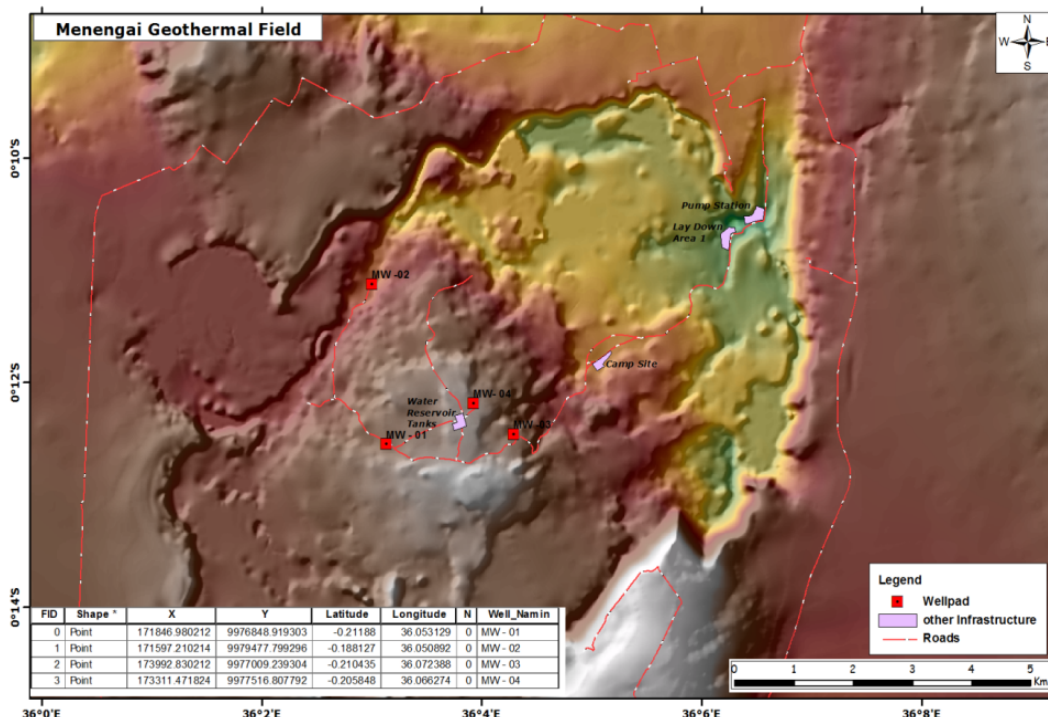

FID	Shape *	X	Y	Latitude	Longitude	N	Well_Nam in
0	Point	171846.980212	9976848.919303	-0.21188	36.053129	0	MW - 01
1	Point	171597.210214	9979477.799296	-0.188127	36.050892	0	MW - 02
2	Point	173992.830212	9977009.239304	-0.210435	36.072388	0	MW - 03
3	Point	173311.471824	9977516.807792	-0.205848	36.066274	0	MW - 04

FIGURE 10: Locations of MW-01 and MW-02 on the Menengai caldera floor (GDC, 2010)

4.2 Drilling wells MW-01 and MW-02

Wells MW-01 and MW-02 are both located on the present day caldera floor with coordinates Eastings 171846.98 and 171597.21, respectively, and Northings 9976848.91 and 9979477.79, respectively. MW-01 was drilled at 2051 m a.s.l. (above sea level) near the central part of the caldera, whereas MW-02 is at a slightly lower elevation of 1894 m a.s.l. at the western end of the caldera (Figure 10). Both wells are vertical to measured depths of 2206 m (MW-01) and 3200 m (MW-02) below ground level. They both targeted in-situ permeable structures, conduits for hot geothermal fluids at depth. MW-01 is situated right on the low-resistivity anomaly, indicated by the surface geophysical exploration, to ascertain the nature and depth of the reservoir. MW-02 was located by the western promontory fault (Figure 5) with the aim of establishing the extent of the caldera resistivity anomaly to the west (Figure 6). In addition, both wells have exposed the underlying lithology and stratigraphy for the first time in this part of the central Kenya rift valley.

The drilling process for both wells was entirely blind as no data were available on the geological structures of the underlying rock formations. This accounts for more operational days than is necessary when drilling in known geothermal areas like Olkaria. MW-01 took 79 days while MW-02 took 125 days (Figures 11 and 12). Much of the drill time was consumed by frequent caving in of numerous weak zones combined with circulation losses. The drilling programme of both wells was divided into 4 stages as highlighted in Tables 1 and 2. Subsequent phases were telescopic from the earlier phases, due to reduced drill bit diameters to the bottom of the well. Surface casing, anchor casing, production casing and slotted liners sequentially characterised the pre-drilling phase, phase 1, phase 2 and phase 3, respectively (Tables 1 and 2).

As shown by Figures 11 and 12, the drilling programmes ran concurrently with MW-01 commencing on 12th of February, 2011, and MW-02 on 28th of February, 2011. Different circumstances were encountered in the two wells.
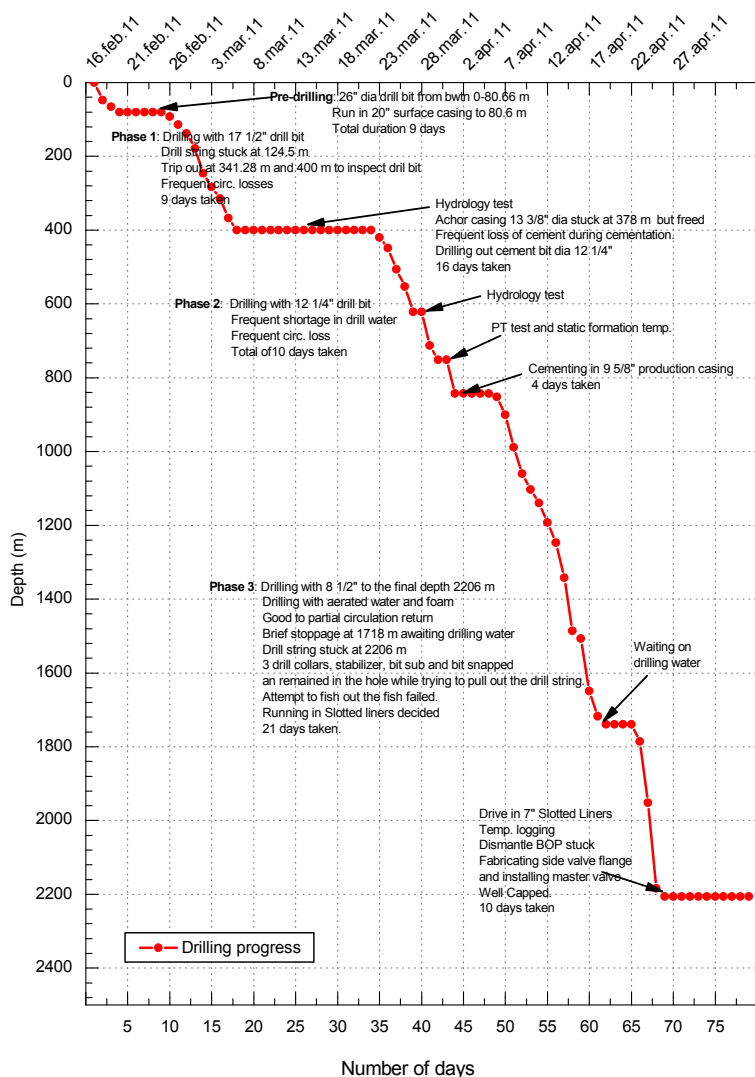

FIGURE 11: Drilling progress for well MW-01

The pre-drilling stage of MW-01(12th Feb. 2011 - 20th Feb. 2011) involved mud and/or water drilling of a 26" diameter hole from the surface to 80.66 m depth and it was dominated by complete circulation losses between 39.35 m and 80.66 m. A 20" diameter surface casing was run in the hole with the casing shoe at 80.6 m. The casing was set with 43.93 tonnes of cement followed by pumping

and backfilling, installation of a casing head flange, a blow-out preventer, a flow line, making a BHA assembly and pressure testing the BOP. All these activities were completed in 9 days of active operation.

Phase 1 of MW-01 (21st Feb. 2011 - 17th March 2011) involved 17½" diameter drilling through the cemented section then in an open hole from 80.66 to 400 m. Occasional cave-ins on pull out of hole (POOH) led to reaming out the collapsed wall materials, a hydrology test at 400 m, running in 13⅜" anchor casing and cementing to the casing shoe depth of 400 m. Six backfills, totalling 101 tonnes, of cement slurry were required with variable densities. This phase lasted for 25 days.

Phase 2 lasted 10 days, between March 18th and March 31st 2011. During this period, a 12¼" hole was drilled through the cement and open hole from 400 to 843 m. A hydrology test was performed at 622 m as was a static formation temperature test at 752 m. Running in of the 9⅝" production casing to the shoe bottom at 843 m followed and subsequently 3 backfills of 27.3 tonnes of cement slurry were pumped.
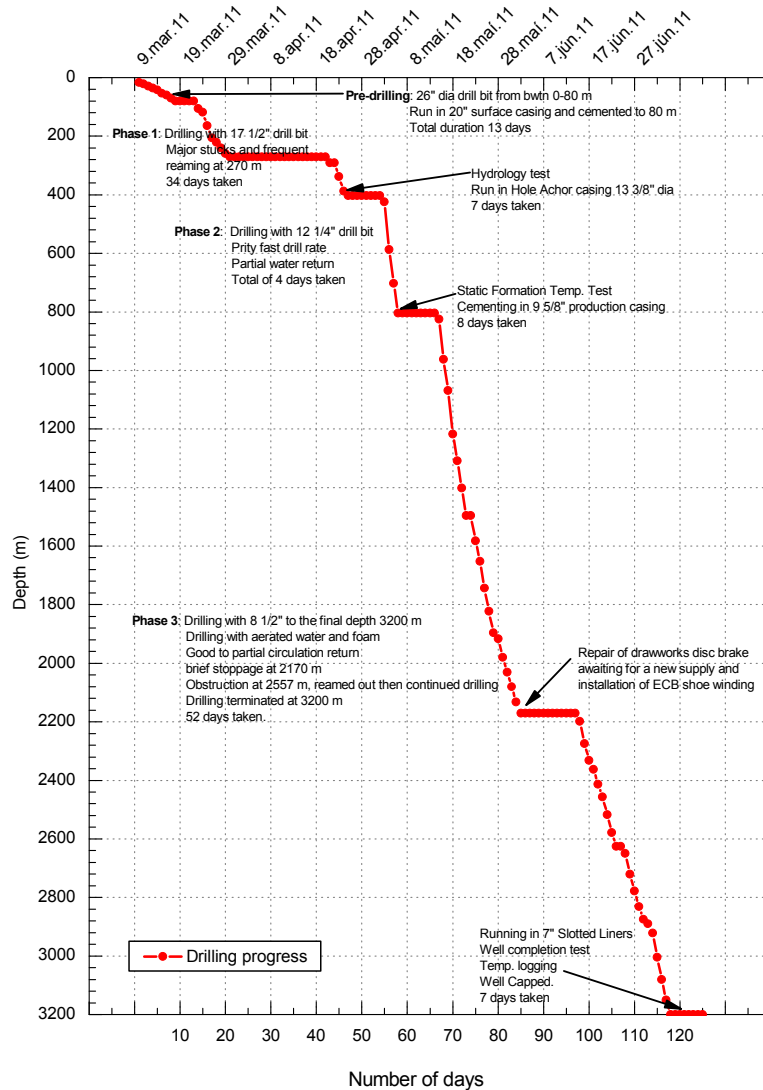
FIGURE 12: Drilling progress for well MW-02

TABLE 1: MW-01 drilling data

Drilling phase	Drilling bit (")	Drilled depth (m)	Casing size (")	Casing shoe (m)
Pre-drilling	26	80.66	20	80.6
Phase 1	17$^1/_2$	400	13$^3/_8$	400
Phase 2	12$^1/_4$	843	9$^5/_8$	840
Phase 3	8$^1/_2$	2206	(7" slotted liner)	(bottom of liner at 2206 m)

TABLE 2: MW-02 drilling data

Drilling phase	Drilling bit (")	Drilled depth (m)	Casing size (")	Casing shoe (m)
Pre-drilling	26	80	20	80
Phase 1	17$^1/_2$	403	13$^3/_8$	403
Phase 2	12$^1/_4$	805	9$^5/_8$	800
Phase 3	8$^1/_2$	3200	(7" slotted liner)	(bottom of liner at 3200 m)

Phase 3 involved making a slick hole of 8½" diameter from 843 m to the bottom of the well at 2206 m. The cement tag was drilled first from 809.2 m to 843 m before proceeding with an open hole to 2206 m, with a brief stop at 1739 m waiting for drilling water. The drill string got stuck at 2206 m and a pull out of hole resulted in a fish, consisting of 3 drill collars, stabilizer, bit sub and the drill bit at 2172.44 m; these were left in the hole since fishing them out never succeeded. Slotted liners were therefore run in the hole; then a completion temperature test was performed. The phase was terminated by breaking and laying down the singles, dismantling the stuck BOP, fabricating a side valve flange, installing the master valve and subsequently capping the well. This phase lasted 31 days between 1st of April, 2011 and 1st of May, 2011.

The MW-02 operations lasted 125 days from the 28th of February 2011 to the 2nd of July, 2011. The final depth was 3200 m. MW-02 also underwent four phases of operations: pre-drilling, phase 1, phase 2 and phase 3 (Figure 12).

Pre-drilling commenced with a well spud on the 28th of February, 2011, with 26" diameter mud drilling from 0 to 80 m. A total loss of circulation was encountered at 43.28 m. Next was the installation and cementing of a 20" casing by pumping in 19.4 tonnes of cement slurry. This operation took a total of 13 days.

Phase 1 involved the drilling of a 17½" hole from 80 to 270.82 m. This was the most problematic phase which lasted 41 days. A brief total loss was encountered at 86.4 and 206.5 m with a brief string stuck at the latter depth. The string also briefly stuck at 213 m resulting in a back off of the Kelly spinner. Total circulation loss occurred between 213 and 270.82 m. Trip in the hole was executed while waiting for drilling water. Meanwhile, it was established that 5 joints of string had their threads damaged due to rotary table limit set at 10 KN.M which was higher than the torque range of the weakest member of the drill string/pipe which was 5-6 KN.M. The string was freed after several reaming attempts with an overpull average of 1800 KN force.

Reaming was continued with aerated water and foam but another tag obstruction was encountered at 99 m. Some LCM of grass, rocks, bentonite bags and sand were dropped in. A cement plug was made by pumping 5 m^3 of neat cement at a slurry density of 1.7 kg/m^3. There was a wait on the cement for 8 hrs and then another 5 m^3 of neat cement at slurry density of 1.7kg/m^3 were pumped. There was a run in hole which tagged top of cement at 88 m, and another cement plug to heal the loss zone at 86 m. 5 m^3 of cement at slurry density of 1.7 kg/m^3 were pumped after dropping grass, rocks, sand, and bags of bentonite. Next was a run in hole with a slick bottom hole assembly, cement was tagged at 79 m, then drilled. At 99 m, just at the bottom of the cement plug, circulation was completely lost and high torque was experienced. The hole was reamed to 139 m and gained circulation returns though persistent high torque. An overpull of up to 2000 KN was exerted to free the string after several failed attempts. Then, 12 m^3 of a cement slurry plug of 1.71 kg/m^3 were pumped in and tagged at 138 m then drilled to 221 m. Reaming proceeded successfully from 221 m to a depth of 270 m. A 17½" diameter hole was drilled from 270 to 403 m. A hydrology test was then conducted at 403 m, followed by the installation of a 13⅜" anchor casing. Here seven backfills totalling 99.72 tonnes of neat cement and slurry with variable densities were consumed.

Phase 2 of MW-02 included drilling coverage of a 12¼" hole from 403 to 805 m depth with aerated water and foam, encountering partial drill water return. A static formation temperature test was performed at 805 m followed by the installation of a 9⅝" production casing with the shoe set at 805 m. Here, 26.5 tonnes of blended casing cement were used with an additional four backfills, amounting to 55 tonnes of clean cement and slurry. This phase was completed in 12 days.

Phase 3 involved drilling an 8½" diameter hole from 805 to the final depth of 3200 m with aerated water and foam, largely with good circulation returns. There was a brief stoppage at 2170 m during repair of the draw works disc brake and the acquisition of a new ECB winding. Slotted liners were

installed from 805 to 3200 m. A well completion test and capping completed the operations of this phase on the 59th working day.

4.3 Stratigraphy of MW-01 and MW-02

Wells MW-01 and MW-02 cut through peralkaline trachytic rocks which may have been formed by fractionation of basaltic magmas via metaluminous trachytes which, in turn, generated pantellerites by the same mechanism. Comenditic rhyolites may have formed from volatile-induced crustal anatexis and may have, themselves, parented the pantelleritic melts through crystal fractionation (Macdonald and Scaillet, 2006). Trachytes range in composition from metaluminous to peralkaline and from silica-oversaturated to silica-undersaturated, while rhyolites range from comendite to pantellerite (Figure 13).
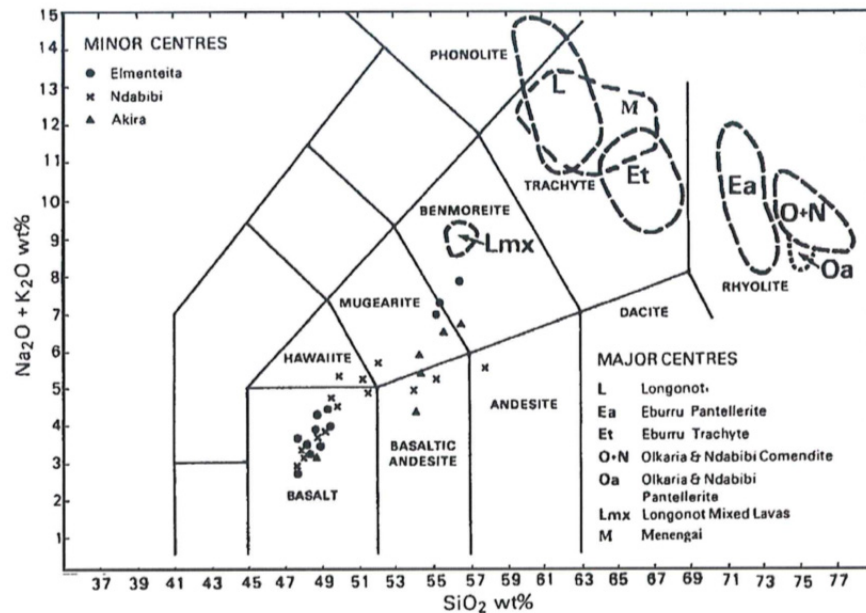
FIGURE 13: Alkali-silica plot showing the compositional range of neighbouring volcanic centres; Menengai (M) rocks are largely trachytic (Macdonald and Scaillet, 2006, modified from Clarke et al., 1990)

Macdonald (1974) classified Menengai rocks based Al_2O_3 and $FeO_{(T)}$ (Figure 14) as ranging from comenditic trachyte through pantelleritic trachyte to pantellerite.
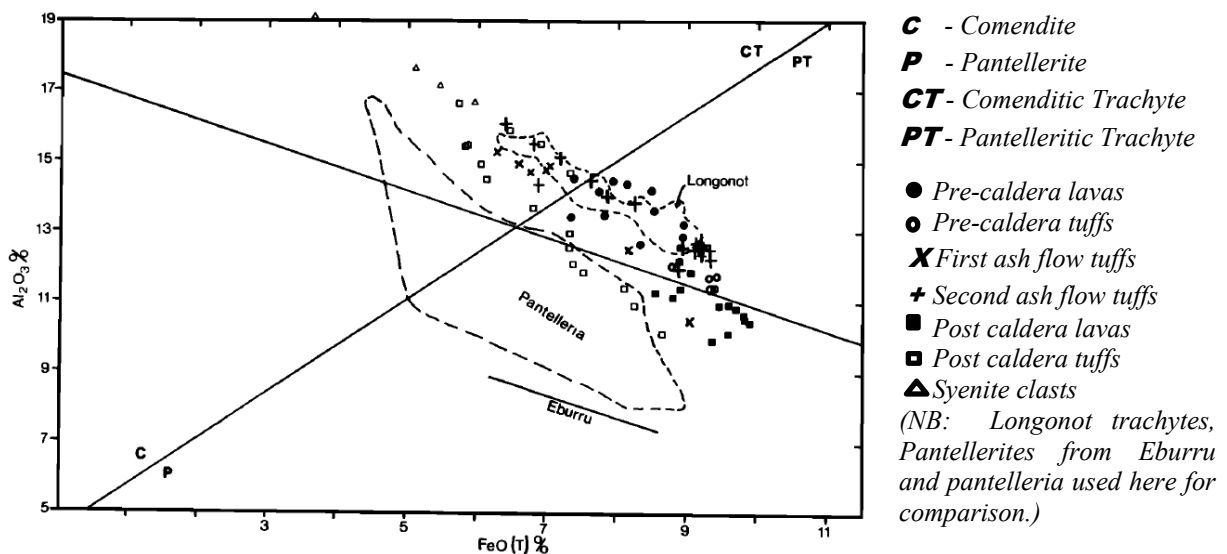
FIGURE 14: Classification scheme for the Menengai per-alkaline, quartz-normative extrusive rocks (Leat et al., 1984; modified from Macdonald, 1974)

4.3.1 MW-01

MW-01 cuts through thick fresh fine- to medium-grained post caldera lavas of pantelleritic trachytes with minor intercalations of tuffs at some depths (see below). A thick pantelleritic intrusion is found between 850 and 1082 m. The intrusion is massive with practically the same mineralogical assemblage, indicative of a generally homogenized lava composition. MW-01 rocks are strongly silica saturated hypocrystalline fine- to medium-grained plagioclase phyric with clinopyroxene aegirine-augite-hedenbergite and amphibolic arfvedsonite-riebeckite microphenocrysts in a microlitic alkali feldspar-rich glassy matrix with scattered specks of iron oxides. The description of the rock formations observed in MW-01, aided by petrographic thin-sections analysis, follows. Hydrothermal clay minerals were barely encountered by XRD analysis except for small amounts of illites (Appendix I). Figure 15 shows the lithology, alteration stage, intrusions, feed zones and temperature logs of well MW-01, as analysed in this study.

0-8 m: *Glassy pantelleritic trachyte*. Greenish-grey, fine-grained, abundant glassy and pumiceous obsidian fragments. Largely greenish tinted by the minor clinopyroxene crystals impregnated in a feldspar-rich matrix.

8-22 m: *Fine-grained pantelleritic trachyte*. Light to dark greenish-grey, hypocrystalline fine-grained felsic rock, feldspar phyric matrix. Iron oxide precipitates are observed at the margins and interstices of clinopyroxene mafic crystals.

22-84 m: *Medium-grained pantelleritic trachyte*. Brown to greenish-grey, hypocrystalline medium-grained with trachytic texture. Feldspar-rich groundmass showing lamellae crystal shape. Porphyritic with minor plagioclase feldspar phenocryst growths in the matrix. Euhedral greenish-yellow pleochroic aegirine-augite is found and hedenbergite clinopyroxene microlites are scattered in the groundmass. Minor amphibole of dark bluish subhedral prismatic riebeckite crystals is evident in fibrous aggregates. Opaque iron oxides are interstitially placed between feldspars. Moderately fractured with a circulation loss zone between 38 and 80 m. Vein fillings of clayey material are found at 80-84 m.

84-122 m: *Fine- to medium-grained pantelleritic trachyte*. Light greenish-grey, fine- to medium-grained hypocrystalline trachytic rock. Plagioclase phenocrysts are scattered in needle like lath shaped euhedral to subhedral alkali feldspar crystals. Abundant opaque iron oxides, appearing brown to deep brown, precipitate between crystals in the groundmass. Prismatic yellowish-green clinopyroxene microphenocrysts and bluish riebeckite crystal are seen in crossed polars.

122-172 m: *Very fine-grained pantelleritic trachyte*. Light greenish grey very fine-grained lava flow. Feldspar rich matrix showing albitic twining. Iron oxide precipitation to dark brown patches. Greenish clinopyroxene aegirine-augite and bluish riebeckite crystals are present.

172-400 m: *Medium-grained pantelleritic trachyte*. Brown-greenish grey medium-grained largely fresh porphyritic and highly fractured section. Plagioclase phenocrysts and aegirine-augite microphenocrysts are scattered within the microlitic alkali feldspar groundmass. Quartz crystal seems to be growing on the fracture zones. Iron oxide precipitates are also evident. Circulation losses were very heavy in this zone, hence no drill cuttings exist at 172-178, 180-192 and 196-400 m.

400-450 m: *Fine- to medium-grained pantelleritic trachyte*. Light greenish-grey fine- to medium-grained fresh porphyritic rock. Plagioclase phenocrysts impregnated in the silica saturated feldspar rich groundmass. Scattered microphenocrysts of yellowish-green aegirine-augite crystals are present, reddish brown iron oxide precipitates at the edges of feldspar crystals and bluish pleochroic amphiboles of minor arfvedsonite-riebeckite assemblages are found. The rock is less fractured than above with no hydrothermal alteration minerals observed. Good circulation returned during the drilling process.
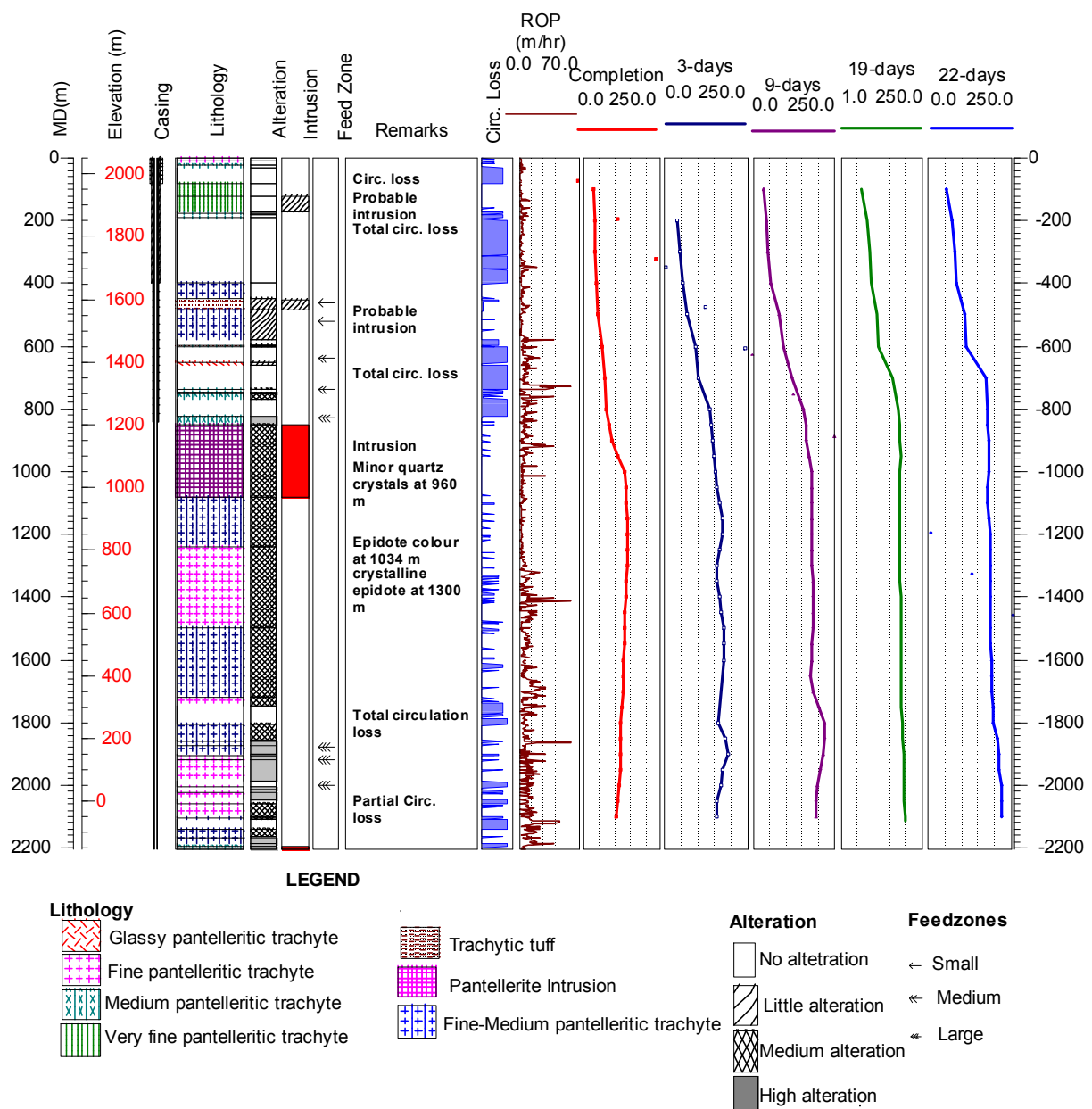
FIGURE 15: Lithology, alteration stage, intrusions, feed zones and temperature logs of well
MW-01 (temperature logs show recovery temperatures taken at completion of drilling,
and after 3, 9, 19 and 22 days upon completion)

450-484 m: *Trachytic tuff.* Reddish brown fine-grained hypocrystalline tuffaceous matrix. Euhedral
plagioclase phenocrysts and minor subhedral aegirine-augite microphenocryst crystals partly embayed
and skeletal in the groundmass which is composed of subparallel microcrystalline needle-like alkali
feldspars. Reddish brown iron oxide precipitates observed between the matrix crystals which are
intersertal, intergranular and subophitically aligned. Minor coronal zonation is seen around the augite,
and radiating quartz crystals indicating mild alterations. The rock has minor calcite and rare
clinopyroxenes and amphiboles. Good circulation return.

484-600 m: *Fine- to medium-grained pantelleritic trachyte.* Pale greenish-grey, fine- to medium-
grained hypocrystalline plagioclase-phyric with minor subhedral aegirine-augite microphenocrysts,
partly skeletal and embayed in subparallel interstertial, intergranular and subophitic rectangular lath-
shaped alkali feldspar-rich groundmass. Minor pyrites, primary quartz and glass fragments. Calcite
and iron oxides are found in the matrix. No circulation losses were encountered in this zone.

600-850 m: *Medium-grained pantelleritic trachyte.* Reddish-brown green to medium-grained hypocrystalline porphyritic silica saturated rock. Euhedral plagioclase phenocrysts and subhedrally zoned embayed aegirine-augite microphenocrysts impregnated in variolitic/divergent needle like lath-shaped feldspar-rich groundmass showing trachytic orientations. Glass and iron oxides interstitially placed between the feldspar crystals. Increased albite twinning of feldspar and partly altered with increasing depth and, at times, wholly altered by calcite. Interstices filled by dark brown oxidised glass and minor clayey materials. Circulation loss from 622-752 m. Increased amount of pyrite crystals indicative of permeable zone.

850-1082 m: *Pantellerite intrusion.* Pale greenish medium, equigranular holocrystalline highly silica saturated fresh rock. The matrix is granophyric with no trachytic flow textures observed. Euhedral crystals of plagioclase and yellowish-green clinopyroxene intergrowths in the rock matrix. Pyrite, iron oxides and clayey particles observed in the interstices of crystal. Plagioclase shows slight albitization and, at times, slightly calcitized and increasingly altered with depth. The clinopyroxene is also slightly altered. High albitization of plagioclase could indicate high-temperature alteration in parts of this zone. No circulation loss indicates a massive, compacted intrusion.

1082-1240 m: *Fine- to medium-grained pantelleritic trachyte.* Light greenish grey, fine- to medium-grained hypocrystalline porphyritic rock. Aegirine-augite clinopyroxene microphenocryst crystals common together with plagioclase phenocrysts in the trachytic groundmass. Plagioclase is almost completely altered/albitized whereas clinopyroxenes are zoned at the margins. The rock shows some fracturing, hence the observed partial circulation loss. Epidote colouration is observable, starting at 1100 m and continues with depth.

1240-1500 m: *Fine-grained pantelleritic trachyte.* Greenish-grey, fine-grained hypocrystalline porphyritic highly altered rock. Plagioclase phenocrysts are partially to completely albitized at this depth and are immersed in lath-shaped feldspar-rich trachytic groundmass with embayed aegirine and augite microphenocrysts. Calcite and iron oxide precipitates are interstitially placed. High-temperature crystalline epidote is observed having full crystalline growth at 1300 m indicative of an alteration temperature of 240-250°C (Kristmannsdóttir, 1979). Crystalline secondary hydrothermal quartz specks are observed, especially between 1406-1410 m and at 1452 m. Partial circulation losses were noted here due to minor fractures.

1500-1720 m: *Fine- to medium-grained pantelleritic trachyte.* Dark greenish-grey fine- to medium-hypocrystalline porphyritic largely fractured but trachytic rock. Plagioclase phenocrysts are mostly albitized and aegirine-augite or augite clinopyroxenes are generally embayed in the altered groundmass, rich in feldspars. Increased iron oxide precipitation is observed and the number of pyrite crystals is increasing in the interstices, especially in highly fractured sections. High-temperature minerals include secondary quartz and epidote.

1720-1808 m: *Fine-grained pantelleritic trachyte.* Greenish grey, fine-grained hypocrystalline porphyritic highly altered rock. Plagioclase phenocrysts and the groundmass are very altered and oxidised. Quartz crystals dominate the hydrothermal indicators. There are minor amounts of calcite and pyrite in this zone. Circulation losses were experienced between 1774 and 1802 m.

1808-1900 m: *Fine- to medium-grained pantelleritic trachyte.* Dark greenish-grey, fine- to medium-grained, porphyritic trachyte rock. The mineral assemblage still consists of plagioclase phenocrysts with dominant clinopyroxenes aegirine-augite growths in lath-shaped feldspar needle like groundmass with intersertal, intergranular and subophitic textures. This unit appears massive and fresh and no circulation loss was noted within.

1900-2100 m: *Fine-grained pantelleritic trachyte.* Light greenish-grey, fine-grained trachyte with a marked amount of clayey materials forming as vein fillings between 1900-1926 m. Highly to completely altered/albitized plagioclase phenocrysts are seen in the groundmass which is also highly

altered. Skeletal augite fragments evident. Highly oxidized and calcitized. High-temperature minerals are epidote and, quartz. Minor circulation losses were observed.

2100-2196 m: *Fine- to medium grained pantelleritic trachyte.* Light greenish-grey, fine- to medium-grained. More or less the same mineral assemblage as seen above. Moderately oxidized and hydrothermally altered. Epidote and crystalline quartz are the main high-temperature minerals observable.

2196-2206 m: *Medium-grained pantelleritic trachyte.* Dark greenish-grey medium-grained hypocrystalline porphyritic trachyte. Plagioclase phenocrysts almost completely albitized and alkali feldspars are oxidized and altered. Clinopyroxenes show coronal zoning and are frequently embayed. Quartz and epidote are the hydrothermal minerals indicative of a high-temperature zone.

4.3.2 MW-02

MW-02 appears to cut through more evolved rocks than does MW-01. The formations seem largely to be rhyolitic trachytes as well as pyroclasts, trachyte, trachyphonolites and a comenditic intrusion at 1952 m. The MW-02 rock series appear physically older than those of MW-01 and must have formed during earlier eruptions. The lithology is highly fractured and has large concentrations of pyrites from the top to the deepest depths, indicating an intensively permeable zone. A description of the cutting analysis down to 2156 m of MW-02, with the help of a binocular microscope, follows. Minor amounts of smectite-illite and mixed layer clays were found by XRD analysis. Figure 16 shows the lithology, alteration stage, intrusions, feed zones and temperature logs of the well, as analysed in this study.

0-10 m: *Pyroclastics.* Brownish-grey mixtures of differentiated fragments composed of volcanic glass, pumice, tuffaceous clayey materials showing high pyritization.

10-86 m: *Rhyolitic trachyte.* Light brownish-grey, fine-grained silica saturated with a mild greenish tint. The rock is porphyritic with plagioclase phenocrysts in a feldspathic groundmass. Abundant primary quartz and minor amounts of clinopyroxene. Oxidation increases with depth. Calcite and pyrite present.

86-194 m: *Pantelleritic trachyte.* Yellow to brownish-green, fine- to medium-grained porphyritic. Phenocrysts are mainly plagioclase and minor microphenocrysts of clinopyroxene. Matrix appears silica-saturated, dominated by feldspars having specks of iron oxides and amorphous silica. Pyrite is absent and a mild calcite presence is observed. Oxidation increases with depth. Circulation was relatively good in most of the section apart from at 86 m where total loss occurred.

194-358 m: *Trachyte.* Greenish-grey, fine- to medium-grained, fractured porphyritic rock. Sanidine phenocrysts in a silica-rich slightly oxidized matrix.

358-652 m: *Trachy-phonolite.* Light greenish-grey, fine-grained showing porphyritic texture with phonolitic splitting flakes. Sanidine phenocrysts are observed patched in a fine-grained groundmass composed of silica-poor and greenish needle like clinopyroxene, giving the rock a green tint. Amorphous silica is seen filling the minor vesicles and pores. Partial loss of circulation was observed during drilling. The formation is dominated by pyrite crystals.

652-1098 m: *Pantelleritic trachyte.* Yellowish to greenish-grey, fine- to medium-grained sanidine phyric. Silica-saturated groundmass with dark green prismatic crystals of clinopyroxenes and has a high concentration of metalliferous vitreous grains and is continually pyritized. Obsidian fragments and pyroclastic intercalations are seen at the contact with the overlying rock. The formation appears fresh. Vein fillings are found at 796-808 m and 852-876 m.
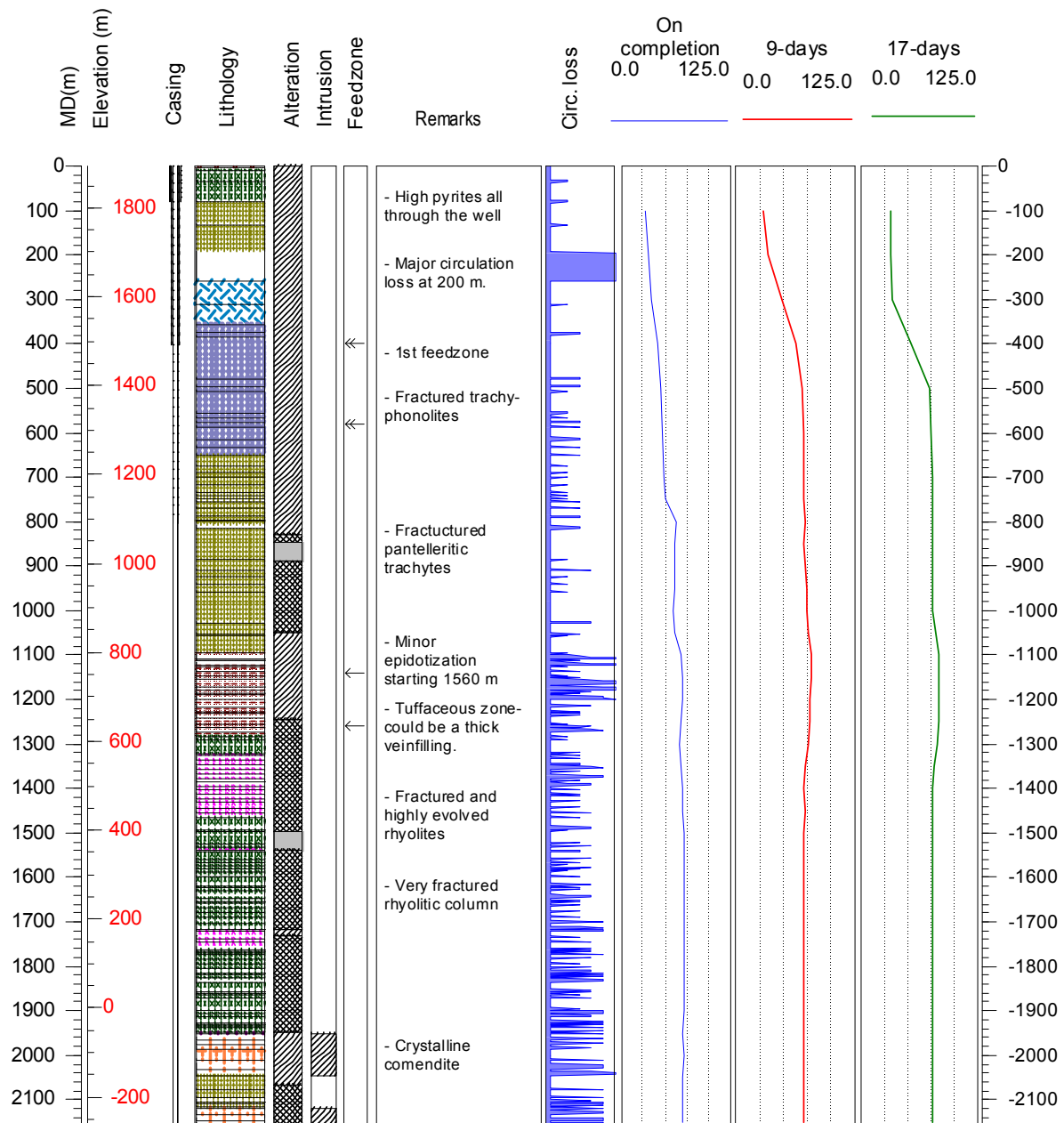
FIGURE 16: Lithology, alteration stage, intrusion, feed zones and temperature logs of well
MW-02 (temperature logs show recovery temperatures taken at completion
and after 9 and 17 days upon completion)

1098-1284 m: *Trachytic tuffs.* Light brownish to yellowish-grey, fine-grained formation. Silica-rich groundmass composed of glass and quartz grains and pumice material. Clinopyroxene is absent and the formation is highly pyritized.

1284-1326 m: *Rhyolitic trachyte.* Brownish grey fine-grained felsic porphyritic highly fractured rock. Plagioclase phenocrysts are impregnated in alkali and a rich feldspar groundmass with minor mafic clinopyroxene.   Partial circulation returns were experienced.   Highly pyritized, oxidised but hydrothermal alteration is minor.

1326-1466 m: *Rhyolite.* Light brownish-grey fine-grained felsic evolved rock. Significant amount of pyrite crystals and the formation is fairly altered. Silica rich matrix showing aphanitic texture. Glassy quartz and feldspars dominate the groundmass, having minor dark iron oxide crystal in the interstices. High pyritization.

1466-1722 m: *Rhyolitic trachyte.* Greyish brown, fine-grained, evolved, fractured and porphyritic rock. Silica saturated matrix with minor mafic clinopyroxenes. Pyrites crystals still dominant.

1722-1762 m: *Rhyolite.* Light brownish-grey, fine-grained fresh granular rock. The matrix is mainly composed of whitish to clear feldspar crystals with impregnation of numerous dark clinopyroxene crystals. Minor epidote colouration starts to appear, indicative of a high-temperature zone. Moderate amount of pyrites. Some circulation losses were experienced during drilling.

1762-1952 m: *Rhyolitic trachyte.* Brownish to dark brownish-grey, fine- to medium-grained highly fractured and oxidised porphyritic rock.   Plagioclase phenocrysts are set in a fine silica-rich groundmass. Minor amounts of epidote were observed between 1784 and 1796 m. Slight circulation losses during the drilling operation.

1952-1964 m: *Comendite.* Light grey, fine-grained, aphyric rock. White glassy feldspar crystalline matrix and scattered dark clinopyroxene specks are seen in the rock. The formation appears as a thick intrusion. Minor amounts of epidotes are observed but they are, however, conspicuously absent in most parts of the formation. Reduced pyritization is observed.

1964-2046 m: *Comenditic trachyte.*   Brownish grey, fine- to medium-grained fractured and plagioclase phyric with siliceous groundmass and minor amounts of clinopyroxene. Some epidote and chlorite observed in the cuttings which are still dominated by pyrite.

2046-2120 m: *Pantelleritic trachyte.* Light greenish-brown, fine- to medium-grained, highly fractured and evolved/reworked rock. Plagioclase phyric and the number of greenish clinopyroxene crystals in the groundmass have increased. Few hydrothermal minerals are found except for possible mixed-layer clays and minor amounts of chlorites at depth. Good circulation returns observed during drilling.

2120-2156 m: *Comenditic trachyte.* Light brownish-grey, fine-grained evolved and a highly oxidised formation.   Porphyritic with plagioclase feldspars forming the main phenocrysts in a fine feldspar microlitic groundmass having minor greenish specks of clinopyroxene.

4.4 Stratigraphic correlations of MW-01 and MW-02

No apparent stratigraphic correlations were observed between the lithologies of MW-01 and MW-02 (Figure 17). The MW-01 formations are largely pantelleritic trachytes with an intrusion between 850 and 1082 m. and another possible intrusion at 2200 m. MW-02 lies within the western promontory fault line and cuts through a mix of fractured evolved rock sequences consisting of pyroclastic, rhyolitic trachyte, pantelleritic trachyte, trachyte, trachy-phonolite, trachytic tuff, rhyolite, comendite and comenditic trachyte. Intrusions and rock formations like those found in MW-01 were never encountered in MW-02.
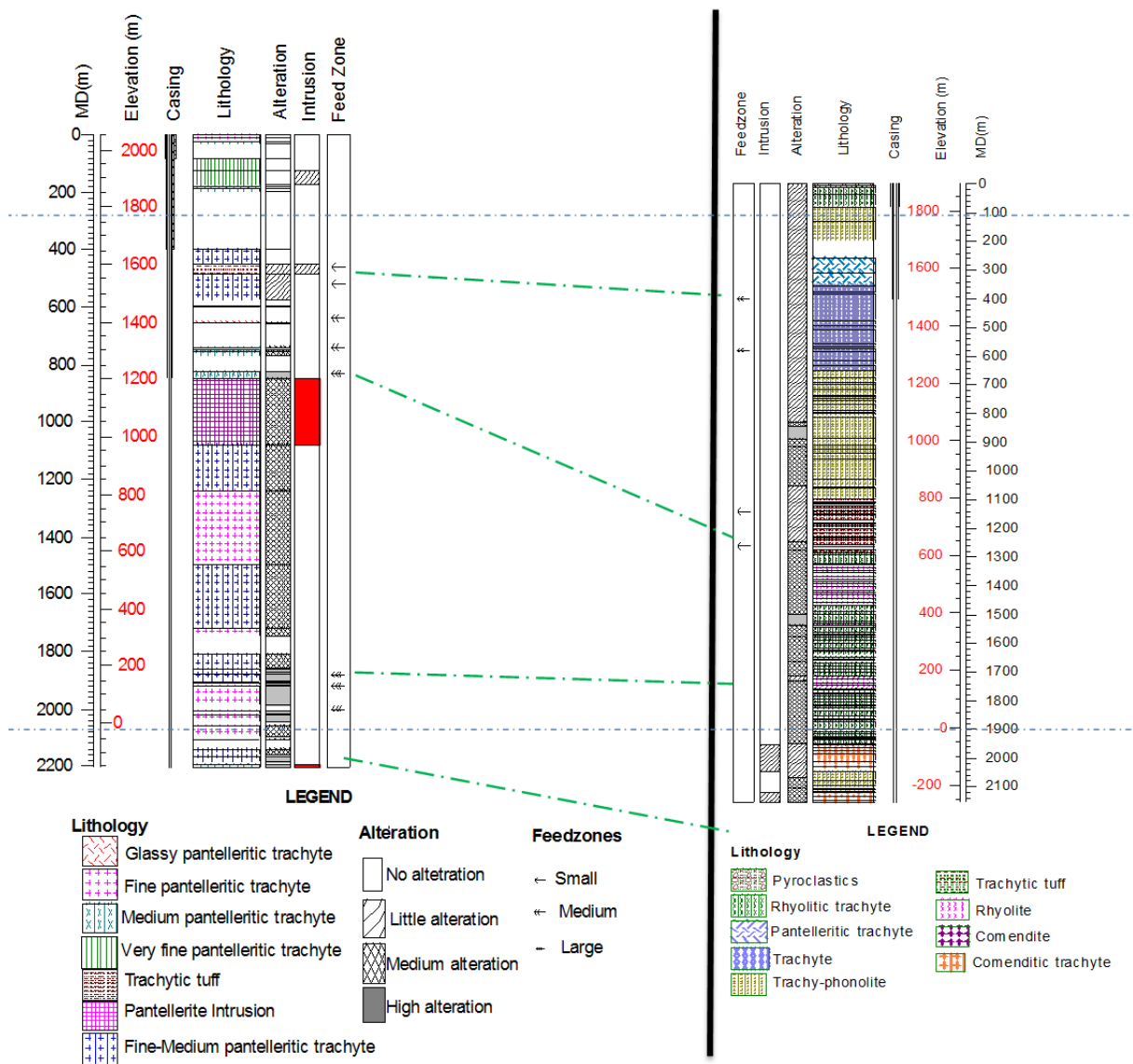
FIGURE 17: Correlation between MW-01 and MW-02

4.5 Intrusions

The main intrusion which was encountered was found in well MW-01 between 850 and 1082 m (Figure 15). However, a medium-grained trachytic formation below 2196 m could also possibly represent an intrusion. In MW-02, no formation could be interpreted as being an intrusive for certain (Figure 16), but a possible intrusion was found at 1952 m depth consisting of a comenditic layer, based on its massiveness and slight trachytic flow textures.

Petrographic analysis of the pantelleritic intrusion in well MW-01 showed an equigranular holocrystalline granophyric massive rock with euhedral plagioclase and clinopyroxene. It did not show any flow texture characteristics, possibly implying a slow magmatic crystallization

4.6 Aquifers and feed zones

Aquifers in both wells were observed in zones shown by changes in the temperature logs. In addition, they were also characterised by an increase in circulation losses of drilling fluid, an increased proportion of high-temperature hydrothermal alteration minerals and changes in penetration rates. MW-01 has two main aquifers at around 800 m and between 1900 and 2000 m. The first aquifer shows an average temperature of 150°C while the second is approximately 200°C. The well column
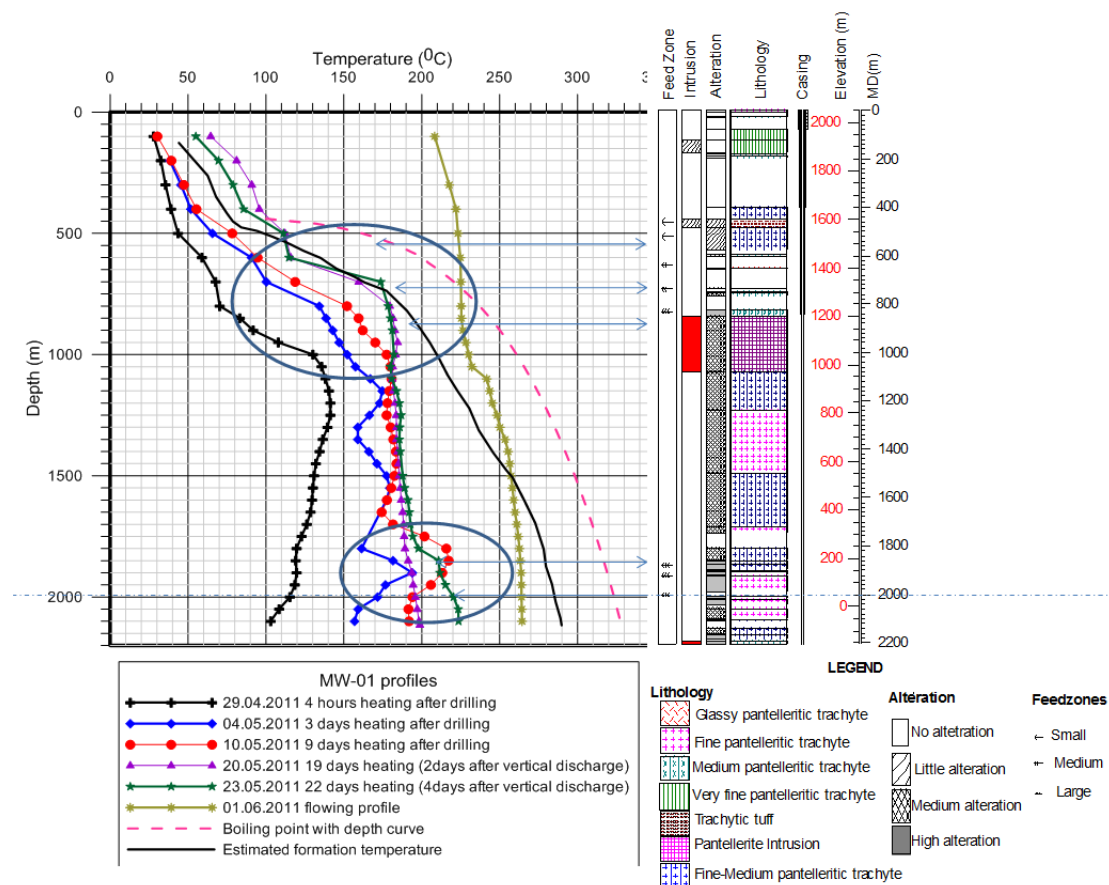
FIGURE 18: Temperature logs and stratigraphy in well MW-01 emphasizing aquifers; circles show increased temperatures indicating feed zone locations

encountered a cold permeable zone between 200-400 m, indicated by total circulation loss (Figure 18). MW-02 encountered aquifers with relatively low temperature (<80°C) at 400-600 m and 1100-1300 m. Four aquifers (Figure 19) were notable at 500 m (~75°C), 1200 m (~80°C), 2300 m (~90°C) and 3200 (~120°C). During this study, well MW-02 was analysed down to 2156 m depth. As described earlier, the well is located right at the western promontory fault, almost at the edge of the caldera floor (Figure 10). The rock formations in the well are heavily fractured and pyritized with partial circulation losses all through the well column. We see a sudden inflow of warm water flowing into the well at 2300 m. We again see increase in temperature at 3100 m, implying a hot geothermal reservoir beneath the massive intrusion.

Feed zones in MW-02 above the production casing will more or less have to be evaluated by circulation losses. Temperature logs show an increase at about 1100 m of slightly hotter water flowing into the well. At about 1300 m, cold water flows into the well and, at about 2250 m, hot water (probably only just above 100°C) flows in and mixes with the cold water. At about 3000 m, the water flows out of the well. The rock formation between 1300 and 2250 m seems relatively cold but significantly hotter below 3000 m.
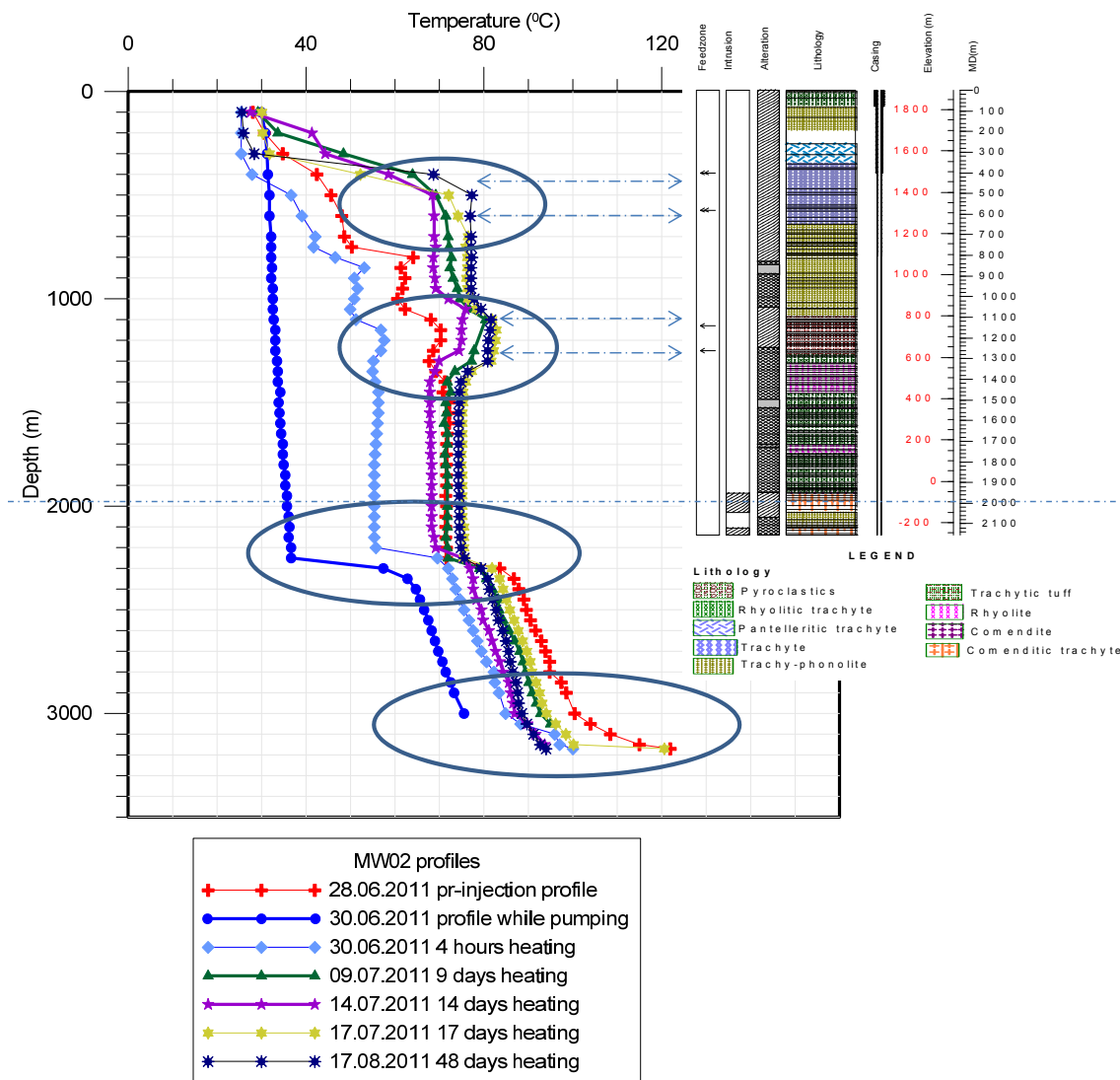
FIGURE 19: Temperature logs and stratigraphy in well MW-02 emphasizing aquifers;
circles show increased temperatures indicating feed zone locations

5. ALTERATION AND HYDROTHERMAL MINERALOGY

Hydrothermal alteration in both wells is largely dependent on the chemical compositions of the rocks along with the temperature, permeability, pressure and hydrothermal fluid and gas compositions. Hydrothermal mineralogical alterations in a geothermal system simply involve the replacement of primary minerals by secondary minerals due to changes in prevailing rock conditions, hence leading to whole rock chemical alteration (Reyes, 2000). Notable alteration minerals in MW-01 include chalcedony, zeolites, quartz, calcite, illite, albite, epidote and pyrite, whereas MW-02 has quartz, minor smectite, minor mixed-layer clays, calcite, illite, epidote and pyrite.

5.1 Primary alteration minerals

The primary minerals in the rocks are unstable at high temperature and pressure and get replaced by more stable minerals depending on the original rock chemistry, permeability and conditions of the hydrothermal agent, in this case water and/or gas (Browne, 1978). Primary minerals present in the

wells include volcanic glass, olivine, pyroxenes, amphiboles, plagioclase, sanidine and iron oxides. Table 3 shows the secondary products of these primary mineral alterations.

TABLE 3: Primary minerals, order of replacement
and alteration products of MW-01 and MW-02

Primary minerals	Secondary mineral products
Volcanic glass, quartz, amorphous silica	Zeolites, quartz, clays, calcite
Olivine	Clay minerals
Pyroxene, amphibole	Illite, pyrite, calcite, clays
Plagioclase	Albite, epidote
Fe-Ti oxide	Pyrite

Volcanic glass, quartz, and amorphous silica: Glass dominates the formation near the surface and parts of some fractures that were encountered in wells MW-01 and MW-02. They form by fast quenching of magmas into glassy obsidian fragments. They exhibit conchoidal cleavages underneath and frequently have brownish oxide tints and oxidation. Primary quartz appears as clear colourless anhedral fragments and alters to give a fully grown euhedral crystal. Amorphous silica occurs as opal or chalcedony, mainly in vesicles, vein fillings and fractures.

Olivine: Olivine is rare in both wells and occurs as greenish glassy crystals. It alters to clays.

Pyroxene, amphiboles: These are relatively abundant in the wells. They do not appear to have undergone total hydrothermal alteration since they are still clearly identified by XRD analysis, as can be seen in the diffractograms in Appendix II. However, those altered have turned to illite, minor pyrites, calcite and very small amounts of clays.

Plagioclase: This is the main type of phenocrysts in the rock assemblage and is easily noticeable in petrographic analysis. It alters largely to albite and epidote.

Fe-Ti oxides: These are the most abundant opaques in the wells and show high resistance to alteration. These oxides occur as ilmenite and magnetite, and alter to pyrite.

5.2 Hydrothermal minerals in MW-01 and MW-02

Hydrothermal minerals are secondary end products from the alteration of primary minerals. As mentioned earlier, they mainly include quartz, calcite, illite, albite, epidote and pyrite. Figures 20 and 21 show the distribution of alteration minerals at depth in wells MW-01 and MW-02, respectively. The main minerals are discussed here below:

Chalcedony: Noted in well MW-01 with a binocular microscope occurring at around 800, 900 and 1100 m. Appears as amorphous silica, colourless, white or bluish-grey, mostly in vesicles, vein fillings or fractures and is characterized by smooth, almost perfectly circular morphology.

Zeolites: Observed at shallow depths (40 m) in well MW-01. These are mainly seen in minor vesicles, having a fibrous shape. They are microporous crystalline solids with well-defined structures. They generally contain silicon, aluminium and oxygen in their framework and cations, water and/or other molecules within their pores (Bell, 2001). They indicate low-temperature alteration (approximately $\leq 120°C$) and typically occur in veins and vesicles.

Illite: Is the main clay mineral in both wells determined by X-ray diffractometry. It replaces K-feldspar and occurs as a vein and vesicle filling mineral. Observed in both wells and is dominant at lower depths (Figures 20 and 21).

FIGURE 20: Lithology and distribution of alteration minerals in well MW-01

Quartz: Euhedral crystalline secondary quartz forms at a minimum temperature of 180°C. It was noted in MW-01 by binocular and petrographic microscope. It appears at greater depths in well MW-02.

Smectite: Conspicuously absent in well MW-01 but is found in minor amounts in MW-02 at 2140 m. In XRD analysis, it shows peaks at 12.93-13.94 Å for untreated samples, 14.1-14.67 Å for glycol treated samples and 10 Å for heated samples.
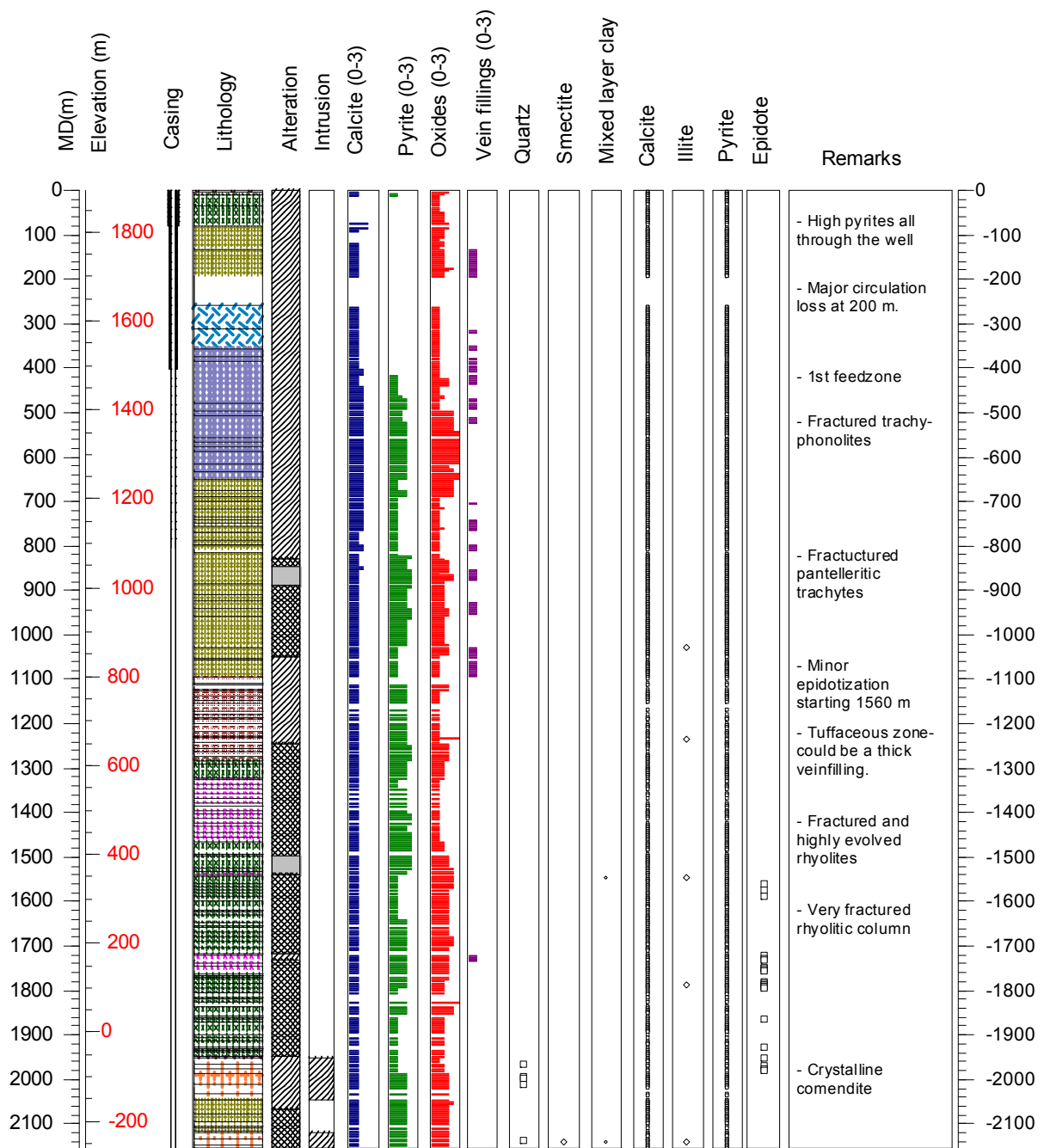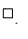
FIGURE 21: Lithology and distribution of alteration minerals in well MW-02

Mixed-layer clays: In minor amounts in MW-02 but absent from MW-01. These were analysed by X-ray diffractometry showing peaks at 13.68-17.4 Å for glycolated samples and values at 7.76-10.14 Å for heated samples (Appendix II).

Calcite: Occurs in almost the entire well columns of MW-01 and MW-02. Appears early in the wells and persists to the bottom. In petrographic analyses, calcite is seen replacing plagioclase phenocrysts.

Albite: Replaces primary K-feldspar and plagioclase phenocrysts. The presence of albite was determined with the use of a petrographic microscope. In MW-01, it is found from 1300 m to the bottom of well. Its presence indicates temperatures above 180°C in a particular formation. Petrographic analysis was not done for MW-02.

Epidote: Is one of the main hydrothermal index minerals. It is a product of hydrothermal alteration of plagioclase, pyroxene and amphiboles. Its presence implies a minimum temperature between 240 and 250°C (Franzson, 2011). The first occurrence of epidote is indicated by colouration and later fully grown yellowish-pale green idiomorphic, tabular, radiate to fibrous crystals. It was observed at 1120 m in MW-01 and its first occurrence in MW-02 was at 1500 m.

Pyrite: Abundant in MW-02 column but sparser in MW-01. It occurs as euhedral cubic crystals with brassy yellow lustre in reflected light. It indicates permeable zones through which hydrogen sulphide gas penetrates.

5.3 Mineralogical evolution and deposition sequences

Petrographic analyses of 40 selected thin sections were used to determine the paragenetic sequence over which hydrothermal evolution occurred. The absence of clear cross-cutting veins and amygdale infillings made it somewhat difficult to establish these sequences. However, the alteration of plagioclase phenocrysts, clinopyroxene microphenocrysts and numerous tabular shaped and acicular groundmass minerals was identified.

In addition, the introduction of high-temperature secondary minerals at depth was taken into consideration in determining the sequence. Overgrowth textures, coronal zonation, skeletal structure and embayment of clinopyroxenes, and albitization and/or calcitization of plagioclase crystals were also noted. Table 4 shows the probable mineralogical deposition and formation sequence in well MW-01.

5.4 Alteration mineral zonation

The degree of alteration, as presented in this study, is based on observations using binocular and petrographic analysis since clay was scarce, as was evident from analysis by the X-ray diffractometer. Minor illite with a peak at 10.1 Å was, however, noted (Appendix II). In Figures 20 and 21 for MW-01 and MW-02, respectively, alterations were graded as none, little, medium or high depending on the physical appearance of the cuttings. Formation temperatures were well defined by minerals having either (OH) or nH_2O in their structures. These included clays, prehnite, zeolite, garnet and amphiboles. A clear cut distribution of these minerals, especially clays (smectite, mixed-layer clay) and chlorite, can give proper information on the alteration zones. Further research is required to determine whether the dominant feldspar and amphibole peaks can be used to define zones in the wells.

5.5 Veins and vesicle fillings

Veins and vesicles dominate the upper sections of the wells and seem to be mainly filled by silica and clayey materials. MW-01 has a bit more of fresh, massive and crystalline homogeneous rocks which rarely contain pore spaces, except in the contact zones of the lava flows. It is at these unconformities that tuffaceous clayey materials intercalate the rock unit (Figure 20). Micro veins and vesicles are,

TABLE 4: Sequence of mineral deposition in well MW-01

Depth (m)	Lithology	Alteration sequence Oldest ⟶ Youngest	Alteration
26	M PT	Zeolite	Little
84	F-M PT		None
108	F-M PT		None
124	V F PT		None
194	M PT	Zeolite	Little
354	M PT		None
430	F-M PT		None
462	T t	Zeolite-calcite	Little
560	F-M PT	Zeolite-calcite	Little
656	M PT	Quartz-pyrite-calcite	None
748	M PT	Pyrite-calcite	None
766	M PT	Pyrite-calcite	Medium
844	M PT	Pyrite-calcite	High
918	P	Quartz-pyrite-calcite	Medium
970	P	Quartz-pyrite-calcite	Medium
1034	P	Quartz-epidote-calcite	Medium
1088	F-M PT	Calcite	Medium
1114	F-M PT	Quartz-pyrite-calcite	Medium
1140	F-M PT	Epidote-pyrite-calcite	Medium
1214	F-M PT	Epidote-pyrite-calcite	Medium
1240	F-M PT	Quartz-pyrite-calcite	Medium
1300	F PT	Albite-quartz-epidote-pyrite-calcite	Medium
1366	F-M PT	Albite-quartz-calcite	Medium
1402	F PT	Albite-quartz-calcite	Medium
1456	F PT	Albite-quartz-calcite	Medium
1494	F PT	Quartz-albite-epidote-calcite	Medium
1522	F-M PT	Quartz-calcite	Medium
1562	F-M PT	Albite-quartz-calcite	Medium
1570	F-M PT	Albite-quartz-calcite	Medium
1590	F-M PT	Albite-quartz-calcite	Medium
1612	F-M PT	Albite-quartz-epidote-calcite	Medium
1626	F-M PT	Albite-quartz-epidote-pyrite-calcite	Medium
1672	F-M PT	Albite-quartz-epidote-pyrite-calcite	Medium
1720	F PT	Albite-quartz-pyrite-calcite	Medium
1854	F-M PT	Albite-quartz-epidote-pyrite-calcite	High
1988	F PT	Albite-quartz-epidote-pyrite-calcite	High
2024	F PT	Albite-quartz-epidote-pyrite-calcite	High
2100	F-M PT	Albite-quartz-calcite	Little
2162	F-M PT	Albite-quartz-epidote-pyrite	High
2206	M PT	Albite-quartz-epidote-pyrite	High

P=pantellerite, V-F PT=very fine-grained pantelleritic trachyte, F PT=fine-grained
pantelleritic trachyte, F-M PT=fine- to medium-grained pantelleritic trachyte,
M PT=medium-grained pantelleritic trachyte, T t=trachytic tuff.

however, evident under petrographic observation to contain glassy amorphous silica material, zeolites, quartz, iron oxide precipitates, calcite, pyrite and minor clays. Well MW-02 probably shows more infilling because it is located in a fracture zone. The rocks are densely fractured and the cuttings are dusty, implying the presence of a large amount of fine rock materials. Veins and vesicle fillings reflect temperature conditions over which the secondary minerals precipitated.

5.6 Fluid inclusions geothermometry

Homogenization temperatures of trapped liquid and gases in clear quartz crystals were measured to determine the formation temperature during their entrapment. Inclusions formed during primary growth (crystallisation) of a mineral are distinct from inclusions incorporated in the host mineral during later processes (recrystallization) after the crystal has been formed (secondary). Shepherd et al. (1985) noted that a general mechanism for forming secondary inclusions involves the development of post crystallization fractures initiated during mechanical or thermal stress. These cracks are then sealed by later fluids to form the characteristic trails of secondary inclusions which typically crosscut earlier generations.
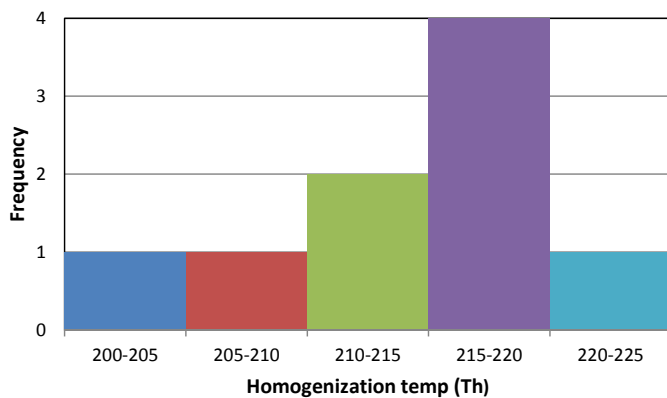
FIGURE 22: Fluid inclusions histogram for MW-01 at 1410 m
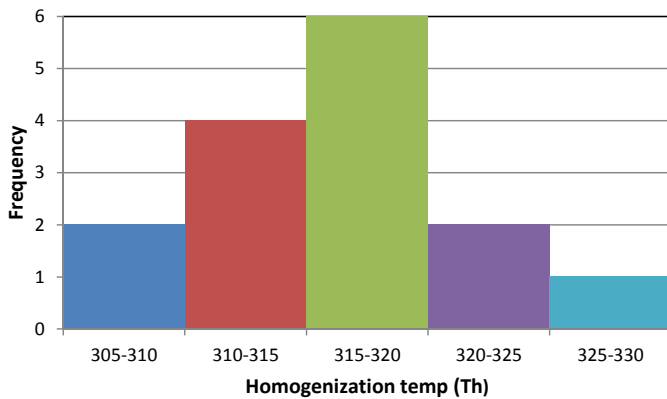
FIGURE 23: Fluid inclusions histogram for MW-01 at 1852 m

The well cuttings were very fine grained and dominated by feldspars that made identification of crystals containing clear fluid inclusion very difficult. However, two quartz crystals were picked at 1410 m and 1852 m depth from MW-01 having 15 and 9 fluid inclusions, respectively (Figures 22 and 23). No crystals could be picked from MW-02. No calcite crystals occurred in either wells for fluid inclusion analysis. Homogenization temperatures (T_h) ranged between 200 and 225°C at a depth of 1410 m and between 300 and 330°C at a depth of 1852 m. The latter had more abundant fluid inclusions. Homogenization temperatures (T_h) were almost identical to the estimated formation temperatures, implying that no major changes, either heating up or cooling, had occurred in the reservoir (Figure 24). The estimated formation temperature curve was derived by averaging the well´s recovery temperature logs with respect to the alteration mineral profile in the well.

Hydrothermal alteration minerals noted in well MW-01 were tabulated according to their first appearance and formation occurrence (Table 5) to give a probable profile of hydrothermal mineral formation. The alteration mineral profile curve showed a progressive temperature increase with depth. Low-temperature minerals such as zeolites formed at shallow depths 20-200 m, followed by calcite (500 m), illite (900 m), quartz (1000 m), and then epidote 1000-2206 m).

A comparison of the measured homogenization temperatures in fluid inclusions with the alteration mineral temperatures and the measured temperature showed that the geothermal system is overall in equilibrium with a reservoir temperature of 200-330°C, increasing with depth. The boiling point curve was generated by the BOILCURV program (Björnsson and Bjarnason, 1993) which calculates the boiling point with depth of a well. The input is the initial depth reference (this may be under or above the wellhead), the depth increment for the calculation and the name of the outfile. Computation is based on the integral formula of pressure that follows the water saturation density with depth.

The homogenization fluid inclusion temperature at 1852 m was 320°C while the estimated formation temperature was 280°C, whereas at 1410 m T_h it was 250°C, lower than the estimated formation temperature of 270°C, implying slight heating.

TABLE 5: Formation tempera-
tures of alteration minerals

Minerals	T_{min} (°C)	T_{max} (°C)
Zeolites	40	120
Quartz	180	300
Calcite	50	300
Illite	230	300
Albite	120	150
Pidote	230	300
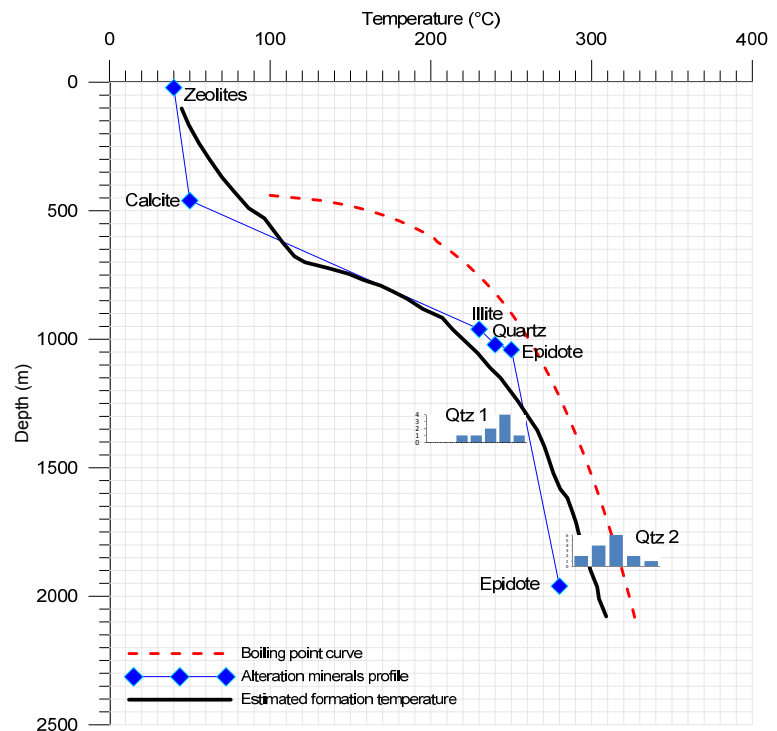
FIGURE 24: Profile of estimated formation temperature,
alteration mineral temperatures and homogenization
temperature in fluid inclusions at 1410 and 1852 m

6. DISCUSSION

Menengai geothermal prospect appears to be influenced by regional and localized structures. The present caldera shows a series of segmental mini collapses within and along fractures which largely influences the permeability of the geothermal fluids. There is a deep intra-caldera lake in the northeast segment of the caldera which appears to act as a local recharge to the geothermal system within the caldera. MW-01 and MW-02 penetrated rocks seemingly formed in different lava eruptions, thereby showing no lithological correlations. MW-01 is located at the centre of the caldera, penetrating a sequence of fresh fine- to medium-grained pantelleritic trachyte which shows compositional zonation and different degrees of gradation. MW-02 is located at the western periphery of the present caldera floor and penetrated more evolved units, largely of rhyolitic trachyte composition with minor phonolitic and comenditic inclusions. The massive volcanic complex is otherwise composed of quartz normative, silica-oversaturated peralkaline trachytes resulting from eruptions tapping highly mixed magmatic chambers.

The drilling project encountered unforeseen hurdles as a result of the lack of prior knowledge of the deep-seated lithology, thereby lasting relatively long periods; MW-01 was completed in 79 days whereas the drilling of MW-02 consumed 125 days. MW-01 encountered an intrusion between 850 and 1082 m and two main feed zones at 600-850 m and 1800-2100 m, and was drilled to a total depth of 2206 m. MW-02 went through a vertical fault line encountering moderately fractured rocks with minor feed zones at 400-600 m and 1100-1300 m. MW-02 was drilled to a total depth of 3200 m. However, this project only covered the top 2156 m of the column. The aquifers/feed zones are associated with lithological boundaries and all lie within the production column fitted by slotted liners in well construction.

The distribution of hydrothermal alteration minerals shows a progressive increase in temperature with depth (Figures 20 and 21). Zeolites and calcites occur at low temperatures while illite, quartz and epidote are the main high-temperature minerals. The absence of high-temperature clay minerals is largely due to the chemical composition of the lithology. Minor smectite and mixed-layer clays noted in MW-02 at 2140 m indicated temperatures of 200°C at the bottom of the well. Illites occurred in both wells in zones believed to have temperatures as high as 200°C. Further research is required to

explain the absence of major clays in this geothermal system and to identify indicators and categories of hydrothermal zones.

Homogenization fluid inclusion temperature (T_h), estimated formation temperature and alteration temperatures in well MW-01 showed no major changes in the reservoir with time. No crystal containing fluid inclusions was identified in MW-02. Permeable zones are characterised by pyritization as they are conduits of geothermal hydrogen sulphide gas which leads to the precipitation of iron sulphides.

7. CONCLUSIONS

Following the observations from this research study, the following conclusions can be made:

1. Present day Menengai caldera is a result of segmental mini-caldera collapses along minor criss-crossing fractures that are now covered by lavas on the post-caldera floor.

2. The existing intra-caldera lake lying underground in the northeast section of the caldera acts as a local recharge to the geothermal system within the caldera.

3. Wells MW-01 and MW-02 do not correlate lithologically. MW-01 encountered post-caldera lavas while MW-02 went through pre-caldera lava sequences. MW-01 cuts through massively fresh silica-saturated peralkaline fine- to medium-grained pantelleritic trachytes with minor intercalations of tuffaceous materials, whereas MW-02 cuts through evolved older rocks of rhyolitic trachyte within phonolitic and comenditic intercalation.

4. The geothermal reservoir beneath Menengai is quite deep (>3,000 m).

5. Probable lateral dyke intrusions exist at the depths of 800-1100 m and 2100-3000 m. These intrusions influence the feed zones in the central part of the caldera. Further mapping of these intrusions in correlation with the findings from wells MW-03 and MW-04 is of essence.

6. Hydrothermal alteration minerals show progressive temperature increase with depth. Low-temperature minerals such as zeolites, calcite and amorphous silica appear first. High-temperature minerals include albite and epidote. The high-temperature system appears below 1300 m in MW-01 and below 1500 m in MW-02. High alteration is indicated by temperatures above 200°C.

7. Comparison of fluid inclusion homogenization temperatures, estimated formation temperatures, and alteration mineral temperatures shows that the geothermal system is overall in equilibrium with an approximate reservoir temperature somewhere between 230 and 280°C.

8. In reference to the circulation loss data, temperature logs and drill cuttings analysis, two main aquifers were notable, between 600 and 850 m and between 1800 and 2100 m in MW-01. It appears that the aquifer between 600 and 850 m is colder and, therefore, gives some cooling effect to the lower aquifer between 1800 and 2100 m. Well MW-02 encountered aquifers between 400 and 600 m, between 1100 and 1300 m, around 2300 m and at 3100 m.

REFERENCES

Arnórsson, S., and Gunnlaugsson, E., 1985: New gas geothermometers for geothermal exploration–calibration and application. *Geochim. Cosmochim. Acta, 47,* 567-577.

Baker, B.H., and Wohlenberg, J., 1971: Structure and evolution of the Kenya Rift Valley. *Nature, 229*, 538-542.

Baker, B.H., Mohr P.A., and Williams, L.A.J., 1972: *Geology of the Eastern Rift System of Africa.* Geol. Soc. of America, Special Paper, 136, 67 pp.

Bell, G.R., 2001: *What are zeolites?* British Zeolite Association, website: *www.bza.org.*

Björnsson, G., and Bjarnason, J.Ö., 1993: *BOILCURV program: ICEBOX geothermal reservoir engineering software for Windows.* ÍSOR, user manual prepared for the UNU-GTP, Iceland.

Browne, P.R.L., 1978: Hydrothermal alteration in active geothermal fields. *Annual Reviews of Earth and Planetary Science, 6,* 229-250.

Clarke, M.C.G., Woodhall, D.G., Allen, D., and Darling G., 1990: *Geological, volcanological and hydrogeological controls on the occurrence of geothermal activity in the area surrounding Lake Naivasha, Kenya, with coloured 1:100 000 geological maps.* Ministry of Energy, Nairobi, 138 pp.

Franzson, H., 2011: *Borehole geology.* UNU-GTP, Iceland, unpublished lecture notes.

GDC, 2010: *Menengai geothermal prospect; an investigation for its geothermal potential.* GDC, Geothermal resource assessment project, unpubl. report.

Jones, W.B., 1985: Discussion on geological evolution of trachytic caldera and volcanology of Menengai volcano, Rift Valley, Kenya. *J. Geol. Soc. London, 142*, 711.

Kristmannsdóttir, H., 1979: Alteration of basaltic rocks by hydrothermal activity at 100-300°C. In: Mortland, M.M., and Farmer, V.C. (editors), *International Clay Conference 1978.* Elsevier Scientific Publishing Co., Amsterdam, 359-367.

Leat, P.T., 1984: Geological evolution of the trachytic caldera volcano Menengai, Kenya Rift Valley. *J. Geol. Soc. London, 141*, 1057-1069.

Leat, P.T., 1991: Volcanological development of the Nakuru area of the Kenya rift valley. *J. African Earth Sciences, 13*, 483-498.

Leat, P.T., Macdonald, R., and Smith, R.L., 1984: Geochemical evolution of the Menengai caldera volcano, Kenya. *J. Geophys. Res., 89*, 8571-8592.

Macdonald, R., 1974: Nomenclature and petrochemistry of the peralkaline oversaturated extrusive rocks. *Bulletin Volcanol., 38*, 498-516.

Macdonald, R., and Baginski, B., 2009: The central Kenya peralkaline province: a unique assemblage of magmatic systems. *Mineralogical Magazine, 73*, 1-16.

Macdonald, R., and Bailey, D.K., 1973: *The chemistry of the peralkaline oversaturated obsidians.* U.S. Geological Survey Professional Paper 440-N-1, N1-N37.

Macdonald, R., Bailey, D.K., and Sutherland, D., 1970: Oversaturated peralkaline glassy trachyte from Kenya. *J. Petrology, 11*, 507-517.

Macdonald, R., and Scaillet, B., 2006: The central Kenya peralkaline province: insights into the evolution of peralkaline salic magmas. *Lithos, 91*, 59-73.

Macdonald, R., Navarro, J.M., Upton, B.G.J., and Davies, G.R., 1994: Strong compositional zonation in peralkaline magma: Menengai, Kenya Rift Valley. *J. Volcanol. & Geothermal Res., 60,* 301-325.

Macdonald, R., Baginski, B., Leat, P.T., White, J.C., and Dzierzanowski, P., 2011: Mineral stability in peralkaline silicic rocks: Information from trachytes of the Menengai volcano, Kenya. *Lithos, 125,* 553-568.

Nehring, N.L., and D`Amore, F., 1984: Gas chemistry and thermometry of the Cerro Prieto, Mexico, geothermal field. *Geothermics, 13*, 75-89.

Ouma, P.A., 2010: Geothermal exploration and development of the Olkaria geothermal field. *Presentation at Short Course V on Exploration for Geothermal Resources, UNU-GTP, GDC and KenGen, Lake Bogoria and Naivaisha, Kenya,* 16 pp.

Reyes, A.G., 2000: *Petrology and mineral alteration in hydrothermal systems. From diagenesis to volcanic catastrophes.* UNU-GTP, Iceland, report 18-1998, 77 pp.

RockWare Inc., 2007: *LogPlot program.* Rockware Inc.

Shepherd, T.J., Ranklin, A.H., and Alderton, D.H.M., 1985: *A practical guide to fluid inclusion studies.* Blackie and Son, Glasgow, UK, 239 pp.

Simiyu, S.M., and Keller, G.R., 1997: Integrated geophysical analysis of the East African Plateau from gravity anomalies and recent seismic studies. *Tectonophysics, 278,* 291-314.

Simiyu, S.M., and Keller, G.R., 2001: An integrated geophysical analysis of the upper crust of the southern Kenya rift. *Geophys. J. Int., 147,* 543-561.

Tongue, J.A., Maguire, P.K.H., and Young, P.A.V. 1992: Seismicity distribution from temporary earthquake recording networks in Kenya. *Tectonophysics, 204*, 71-79.

Young, P., Maguire, P., Laffoley, A., and Evans, J., 1991: Implications of the distribution of seismicity near Lake Bogoria in the Kenya rift. *Geophys. J. Int., 105,* 665-674.

APPENDIX I: Results of the XRD analysis of clay minerals

MW-01			
Sample no.	Depth (m)	Minerals	Remarks
1	16	Amph., feld.	No clays
2	26	Amph., feld.	No clays
3	82	-	No clays
4	112	Amph., feld.	No clays
5	126	Amph., feld.	No clays
6	180	-	No clays
7	312	Feld., illite.	Minor illites clays
8	354	Feld., illite.	Minor illites clays
9	402	Feld.	No clays
10	460	Feld.	No clays
11	500	Feld., amph.	No clays
12	660	Amph., feld.	No clays
13	764	Feld.	No clays
14	826	-	No clays
15	940	Illite	Illites clays
16	1086	Amph., feld.	No clays
17	1212	Amph., feld.	No clays
18	1320	Amph., feld.	No clays
19	1402	Amph., feld.	No clays
20	1440	Amph., feld.	No clays
21	1598	Illite, amph.	Minor illites clays
22	1670	-	No clays
23	1772	Illite, amph.	Minor illites clays
24	1832	Amph., feld.	No clays
25	1908	Illite, amph.,feld.	Minor illites clays
26	1934	Illite, amph., feld.	Minor illites clays
27	2024	-	No clays
28	2108	Illite	Illites clays
29	2156	Illite, amph., feld.	Minor illites clays
30	2204	Illite.	Illites clays

MW-02			
Sample no.	Depth (m)	Minerals	Remarks
1	100	Feld.	No clays
2	418	Feld.,amph.	No clays
3	580	Feld.,amph.	No clays
4	840	-	No clays
5	1030	Illite., amph.	Minor illite clays
6	1236	Illite., amph., feld.	Minor illite clays
7	1546	Illite., mlc., feld.	Minor illite and mixed-layer clays
8	1786	Illite., amph.	Minor illite clays
9	2140	Illite., mlc.,	Illite and mixed-layer clays

APPENDIX II: Characteristic XRD patterns for the clay minerals of wells MW-01 and MW-02

MW-01:

51456/MW-1 #04 OMH

Amphiboles + Feldspars (112 m)
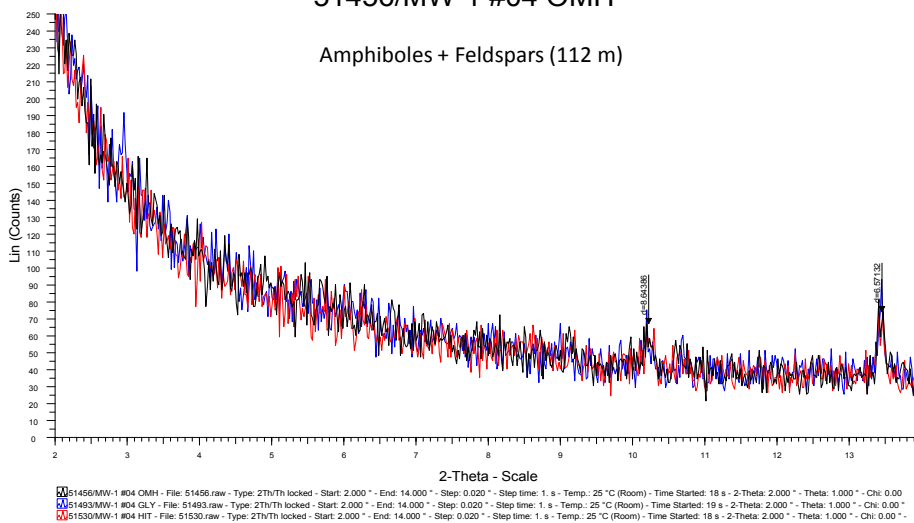
51459/MW-1 #07 OMH

Feldspars + Illite (312 m)
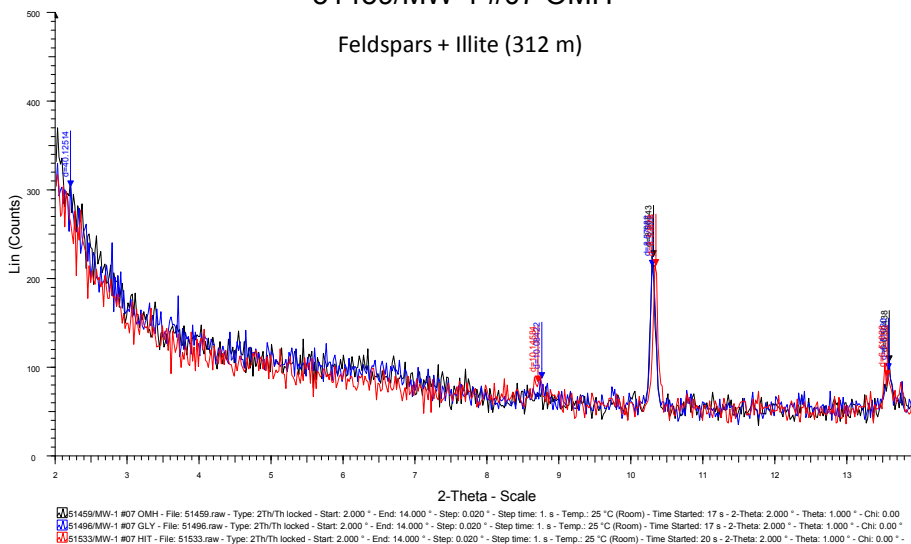
51467/MW-1 #15 OMH

Illite (940 m)
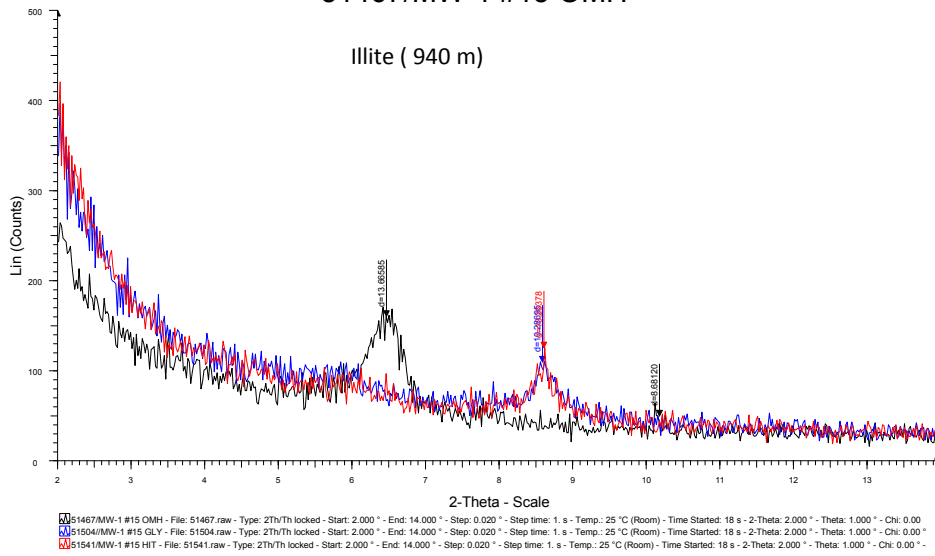
51473/MW-1 #21 OMH
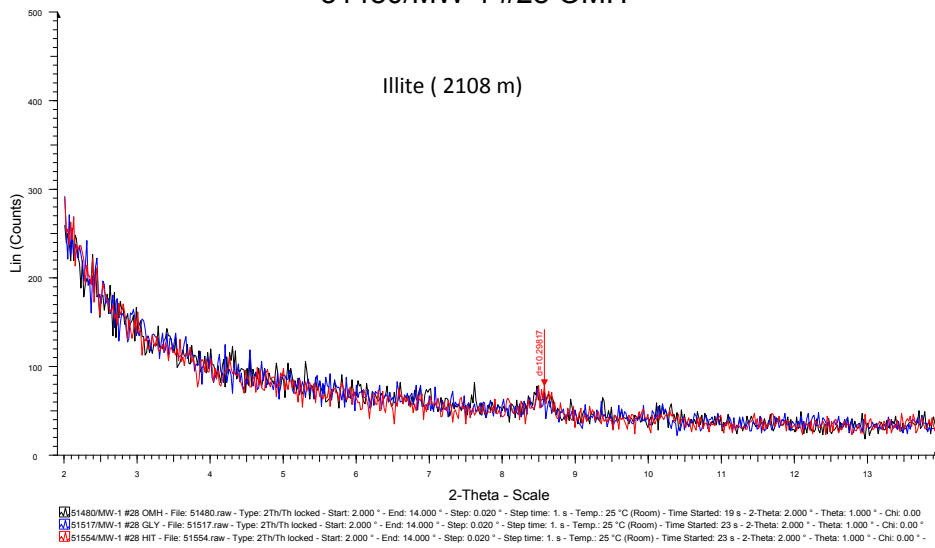
Illite + Amphiboles (1598 m)
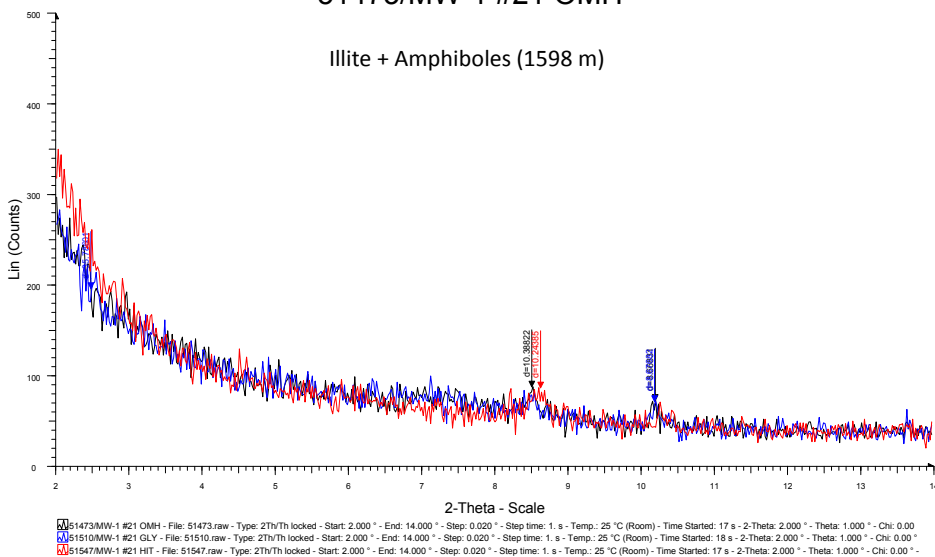
51477/MW-1 #25 OMH
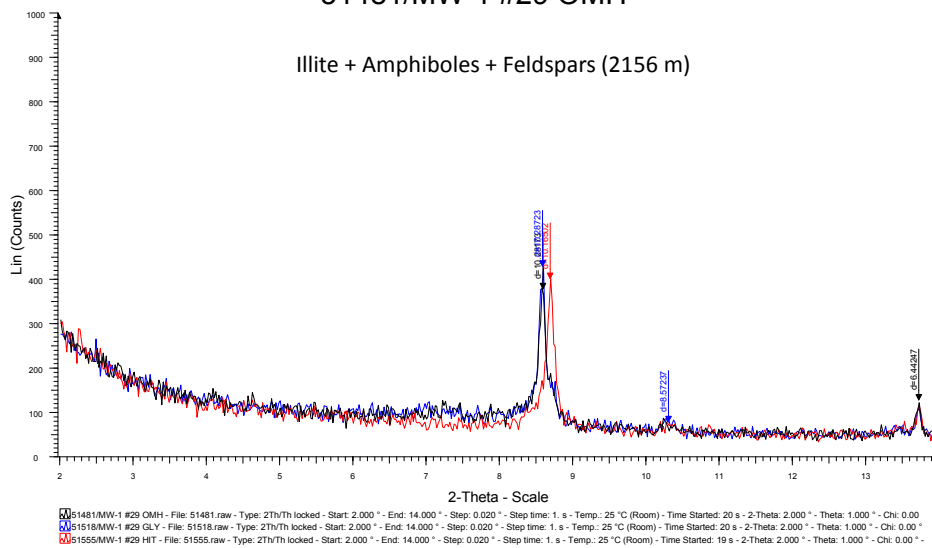
Illite + Amphiboles + Feldspars (1908 m)
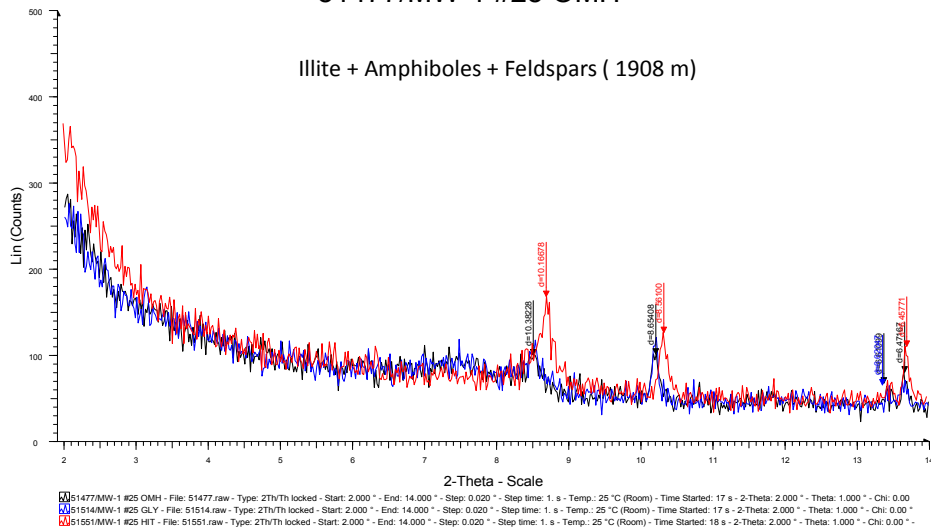
51480/MW-1 #28 OMH
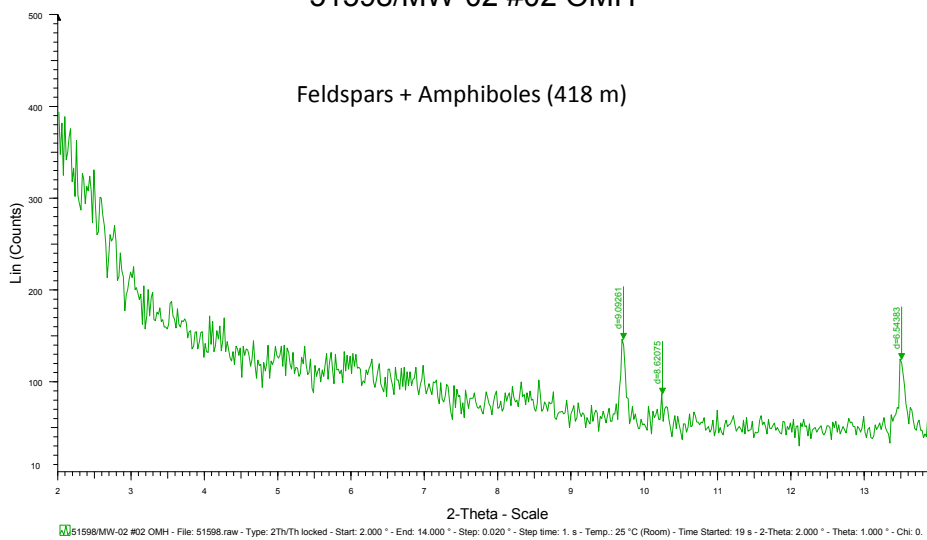
Illite (2108 m)

51481/MW-1 #29 OMH

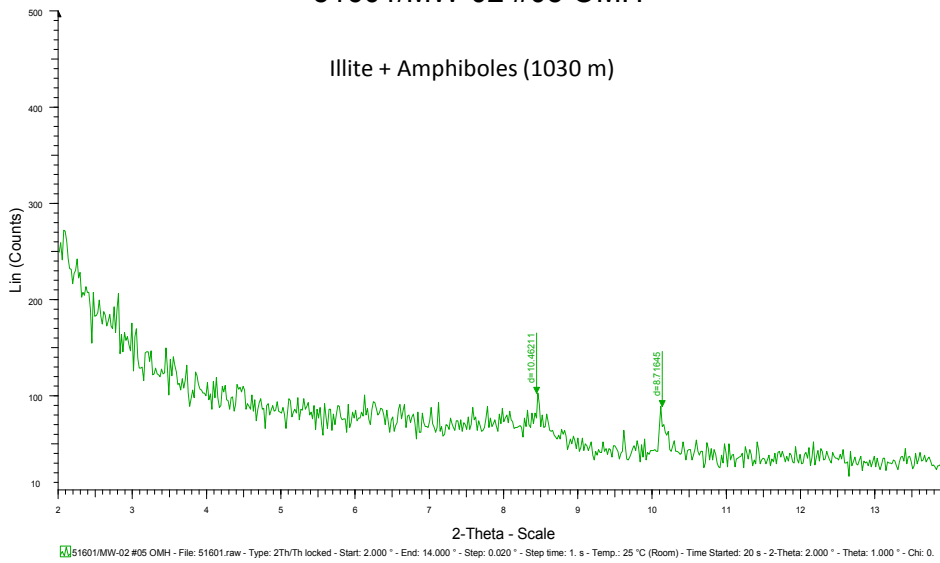Illite + Amphiboles + Feldspars (2156 m)

MW-02:

51598/MW-02 #02 OMH
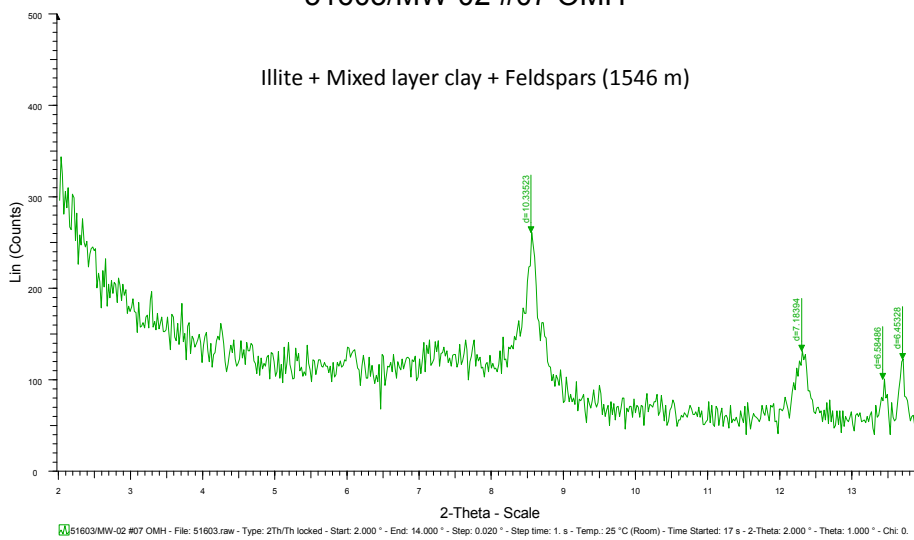
Feldspars + Amphiboles (418 m)

51601/MW-02 #05 OMH

Illite + Amphiboles (1030 m)

51603/MW-02 #07 OMH

Illite + Mixed layer clay + Feldspars (1546 m)

51605/MW-02 #09 OMH

Illite + Mixed layer clay (smectite/chlorite) (2140 m)